Comparative analysis of piRNA sequences, targets and functions in nematodes

Hannah L. Hertz[1,2,†], Benjamin Pastore[1,2,3,†], Wen Tang[1,2*]

[1]Department of Biological Chemistry and Pharmacology.

[2]Center for RNA Biology.

[3]Ohio State Biochemistry Program. Ohio State University, Columbus, OH 43210, USA.

[†] These authors contributed equally to this work.

* To whom correspondence should be addressed: Tel: +1-6142937427; email:

tang.542@osu.edu

ABSTRACT

Piwi proteins and Piwi-interacting RNAs (piRNAs) are best known for their roles in suppressing transposons and promoting fertility. Yet piRNA biogenesis and its mechanisms of action differ widely between distantly related species. To better understand the evolution of piRNAs, we characterized the piRNA pathway in *C. briggsae*, a sibling species of the model organism *C. elegans*. Our analyses define 25,883 piRNA producing-loci in *C. briggsae*. piRNA sequences in *C. briggsae* are extremely divergent from their counterparts in *C. elegans*, yet both species adopt similar genomic organization and transcription programs that drive piRNA expression. By examining production of Piwi-dependent secondary small RNAs, we identified a set of protein-coding genes that are evolutionarily conserved piRNA targets. In contrast to *C. elegans*, small RNAs targeting ribosomal RNAs or histone transcripts are not hyper-accumulated in *C. briggsae* Piwi mutants. Instead, we found that transcripts with few introns are prone to small RNA overamplification. Together our work highlights evolutionary conservation and divergence of the nematode piRNA pathway and provides insights into its role in endogenous gene regulation.

INTRODUCTION

Piwi proteins—members of the Argonaute family—and their piRNA cofactors are found in most of animals [1-3]. Studies from model organisms including *D. melanogaster*, *C. elegans* and mouse have provided key insights into piRNA biogenesis and functions. Genomic origins and sources of piRNAs are remarkably diverse across species. Single-stranded precursor transcripts are generated from piRNA-producing loci and then processed into mature piRNAs. Mature piRNAs are generally 21-35 nucleotides (nts) in length, preferentially start with a 5' Uridine, and possess 2'-O-methylated 3'-ends [1-3]. The Piwi/piRNA pathway plays key regulatory roles in germline development and gametogenesis, hence is required for fertility [4-8]. So far, the best-established function of piRNAs across species is to maintain genome stability by silencing transposable elements in the animal germ line [9-11]. Yet accumulating evidence suggests that piRNAs regulate the expression of some endogenous transcripts and perform species-specific functions [12-17].

With powerful molecular and genetic tools, *C. elegans* becomes one of vital model systems in studying the piRNA pathway. A single functional *C. elegans* Piwi protein, named PRG-1, associate with piRNAs which are referred to as 21U-RNAs due to their strong propensity for a 5'-monoP uridine residue and length of 21-nt [18-22]. Two classes of piRNAs (type I and type II) were discovered [19]. Type I piRNAs are derived from two large clusters on chromosome IV [19-21]. The promoters of many type I piRNA genes contain an 8-nt consensus Ruby motif CTGTTTCA which is associated with chromatin factors including PRDE-1, SNPC-4, TOFU-4 and TOFU-5 [23-26]. Type II piRNA loci lack the Ruby motif and are associated with the promoters of many RNA polymerase II genes [19]. Both type I and II piRNAs are produced from 25- to 29-nt capped small RNA (csRNA) precursors [19]. To generate mature piRNAs, the 5' cap and first two-nts of csRNAs are removed. Additional nucleotides are trimmed from their 3' ends and 2'–*O*–methylation follows [27-30].

In *C. elegans*, most piRNAs lack obvious sequence complementarity to transposons [18-21]. By allowing mismatches, PRG-1/piRNAs recognize hundreds of germline transcripts and recruit RNA-dependent RNA Polymerases (RdRPs) to initiate the biogenesis of secondary siRNAs. These secondary siRNAs show the propensity for 22-nt length and 5' guanine residues, thus are referred to as 22G-RNAs [31-34]. 22G-RNAs are loaded onto worm-specific Argonautes (WAGOs) that maintain and propagate epigenetic silencing [35-39]. Surprisingly, recent studies showed that *C. elegans* piRNA pathway promotes the expression of mRNAs and ribosomal RNAs by preventing unchecked amplification of 22G-RNAs [40-43]. It is unclear whether these observations are specific to *C. elegans* or can be applied to other nematode lineages or across phyla.

To better understand piRNA evolution and function, we characterized the piRNA pathway in *C. briggsae*, a nematode that diverged from *C. elegans* roughly 100 million years ago [44]. By sequencing small RNAs co-purified with *C. briggsae* Piwi protein, we identified 25,883 piRNA-producing loci and found that they are localized to at least three clusters on chromosome I and IV as well as promoter regions genome-wide [45]. We show that piRNAs induce the production of 22G-RNAs which are likely loaded onto WAGOs, but not onto CSR-1 Argonaute which are thought to protect endogenous germline genes from piRNA-mediated silencing [46, 47]. Furthermore, we identified 88 protein-coding genes that are targeted by both *C. elegans* and *C. briggsae* piRNA pathways. Although loss of Piwi leads to transgenerational infertility in *C. briggsae*, we did not detect hyper-accumulation of 22G-RNAs targeting ribosomal RNAs or histone mRNAs as observed in *C. elegans prg-1* mutants [41-43]. Upon loss of piRNAs, 22G-RNAs are overamplified preferentially from the transcripts possessing few introns. Altogether our comparative analyses revealed both conserved and species-specific features in the nematode piRNA pathways.

RESULTS

Identification and characterization of piRNA-producing loci in *C. briggsae*

The nematodes *C. briggsae (Cbr)* and *C. elegans (Cel)* diverged from a common ancestor tens of million years ago [44]. *C. briggsae* expresses a single Piwi protein: Cbr-PRG-1 (WormBase ID: WBGene00032975). Using CRISPR/CAS9 genome editing, we introduced 3xflag sequences to the genomic locus of *Cbr-prg-1*. Western Blotting analysis confirmed the expression of 3xFLAG::Cbr-PRG-1 protein (Fig S1A). To identify piRNAs in *C. briggsae*, we enriched 3xFLAG::Cbr-PRG-1 by immunoprecipitation (IP) and deep-sequenced the co-purified small RNAs, then aligned sequencing reads to the *C. briggsae* genome (WormBase release WS279). From two biological replicates. small RNAs from many distinct genomic loci were significantly enriched in Cbr-PRG-1 IP (IP/input ≥ 4-fold; p-value < 0.05, Two-tailed t-test) (Fig 1A). Similar to their counterparts in *C. elegans*, the majority of Cbr-PRG-1 bound small RNAs are 21 nucleotides in length and exhibit a 5' terminal uridine (Fig 1B). We thus refer to them as 21U-RNAs. Our analyses defined in total 25,883 piRNA-producing loci (Table S1), a number much larger than that previously estimated [45]. We found examples of discrete piRNA-producing loci (Fig S1B) as well as overlapping piRNA-producing loci (Fig S1C). To further validate authenticity of piRNA genes, we generated a presumptive null allele of *Cbr-prg-1* that bears a 5-nt deletion downstream of the start codon and shifts the open reading frame [15]. Consistent with previous findings that the stability of piRNAs and Piwi protein are co-dependent in *C. elegans* [18, 21, 23, 48], the overall abundance of 21U-RNAs in the *Cbr-prg-1* mutant animals was reduced to ~1% of wild-type (Fig 1C).

We assessed the sequence conservation of *Cbr*-piRNAs (n=25,883) and *Cel*-piRNAs (n=15,363) in comparison with the sequence conservation of miRNAs and tRNAs. Consistent with previous findings [45], 0%, 0.01%, 0.04%, and 0.41% of *C. briggsae* piRNAs had potential homologs in *C. elegans* when allowing zero, one, two, or three mismatches respectively (Fig 1D). miRNAs are

~22 nt small RNAs that regulate mRNA stability and suppress mRNA translation in diverse organisms [49]. *C. briggsae* miRNAs (n=131) and *C. elegans* miRNAs (n=368) exhibited stronger sequence conservation as compared to piRNAs. 29.77%, 41.22%, 51.15%, and 54.96% of *C. briggsae* miRNAs had potential homologs in *C. elegans* when allowing zero, one, two, or three mismatches respectively (Fig 1D). The tRNA group displayed strongest sequence conservation among three non-coding RNA categories. 63.19%, 72.33%, 76.71%, and 78.89% of *C. briggsae* tRNAs had homologs in *C. elegans* when allowing zero, one, two, or three mismatches respectively (Fig 1D). These findings indicate that in contrast to miRNAs and tRNAs, sequences of nematode piRNAs are poorly conserved and likely not subject to positive selection.

We next examined the distribution of piRNA-producing genes throughout *C. briggsae* genome. 17,751 piRNA-producing loci were concentrated in three large genomic clusters (9,830,000~12,000,000 on chromosome I, and 18,000~7,140,000 and 13,000,000~15,000,000 on chromosome IV) on both Watson and Crick strands (Fig 1E and 1F) [45]. We also found that 8,132 piRNA-producing loci were widely distributed across the chromosome I, II, III, IV and V, but scarcely present on chromosome X (Fig 1E and 1F). piRNA within the clusters and outside the clusters bore a resemblance to type I and type II piRNAs discovered in *C. elegans* [19]. For example, similar to *C. elegans* type I piRNA genes, *C. briggsae* piRNA-producing loci within the clusters on both chromosome I and IV shared the upstream 8-nt Ruby motif CTGTTTCA (Fig 1F) [20, 45, 50]. In contrast, Ruby motif was not found at the piRNA-producing loci outside of the clusters (Fig 1F). Both types possessed a strong bias for pyrimidine (Y: cytosine/thymine) and purine (R: guanine/adenine) dinucleotide 3- and 2-nt upstream of T which corresponds to 5' end of 21U-RNA. The Y/R dinucleotide is known as the initiator element for RNA Polymerase II transcription initiation [51, 52]. It is thus possible that the transcription of *C. briggsae* piRNA precursors initiate two nucleotides upstream of the 5' end of mature piRNAs. Low melting temperature of the DNA-RNA hybrid induces RNA polymerase II pausing/termination at *C.*

elegans piRNA genes [50]. Consistent with this notion, we found both classes of piRNAs A/T rich motifs downstream of 21U-RNA sequences which might serve as terminator signals (Fig 1F). Finally, it's worth noting that although the number of type I piRNAs is roughly twice as many as type II piRNAs, their overall abundance is ~8-fold higher (Fig S1D). Altogether, our analyses revealed that *C. elegans* and *C. briggsae* piRNA sequences evolve rapidly despite conserved features of promoters and terminators.

C. briggsae TOFU-5 associates with piRNA clusters

The presence of Ruby motif in both *C. elegans* and *C. briggsae* piRNA genes prompted us to test whether the transcription factors are evolutionarily conserved. Prior studies showed that a transcription complex comprised of PRDE-1, SNPC-4, TOFU-4 and TOFU-5 drives the transcription of piRNA precursors in *C. elegans* [23-26]. All four protein factors localize to piRNA clusters and their recruitment is co-dependent on one another [23, 24, 26]. Among them, TOFU-5 is a nematode-specific protein with a SANT domain, a domain that is capable of directly binding to histones [53]. TOFU-5 in *C. elegans* is 76.2% identical to Cbr-TOFU-5 (WormBase ID: WBGene00032059) at the amino acid level (Fig S2). To determine the subcellular localization of TOFU-5, we used CRISPR/Cas9 to generate *C. elegans* and *C. briggsae* strains in which *gfp* sequences were integrated to *tofu-5* genomic loci.

C. elegans piRNA clusters are located at chromosome IV [18, 20, 21]. Consistent with previous findings [24, 26], Cel-GFP::TOFU-5 forms distinct foci at mitotic and meiotic nuclei (Fig 2A and 2B). In particular, two Cel-GFP::TOFU-5 foci were observed in mitotic germ nuclei because of the presence of homologous chromosomes (Fig 2B and 2E). A single Cel-GFP::TOFU-5 focus was observed in each meiotic nucleus because of synapsis of homologous chromosomes (Fig 2B and 2E) [24, 26]. *C. briggsae* piRNA clusters are present on both chromosome I and IV (Fig 1E). If Cbr-GFP::TOFU-5 binds to piRNA clusters *C. briggsae*, it was expected to identify four Cbr-

GFP::TOFU-5 foci at mitotic nuclei and two foci at meiotic nuclei. Imaging by spinning disk confocal microscopy indeed confirmed approximately four Cbr-GFP::TOFU-5 foci per nucleolus in the mitotic zone (Fig 2C and 2E). Surprisingly, a single Cbr-GFP::TOFU-5 focus was detected in nuclei of the meiotic zone (Fig 2C and 2E). One possible explanation is that Cbr-GFP::TOFU-5 binds to the piRNA cluster either on chromosome I or chromosome IV at the meiotic stage. Alternatively, piRNA clusters at chromosome I and IV may be in close proximity in *C. briggsae* meiotic nuclei. Future studies, such as DNA Fluorescence in situ hybridization and super-resolution microscopy, are required to test these models.

To further confirm the association of Cbr-GFP::TOFU-5 with *C. briggsae* piRNA clusters, we generated transgenic animals containing an extrachromosomal piRNA array. In brief, a piece of *C. briggsae* DNA (5,866,040-5,867,890 chromosome IV) containing 21UR-9050, -18460, -1768, -9068, -5728, -11119, -15127, -4796, -3198, -15681, and -4140 genes was cloned. Then it was microinjected into the syncytial gonad of *C. briggsae*, where highly-repetitive and semi-stable extrachromosomal arrays were formed [54]. The transgenic animals were mosaic, expressed the piRNA array in a variable number of cells, and displayed variable transmission rates. In transgenic animals carrying the piRNA array, some mitotic and meiotic nucleic exhibit increased number of Cbr-GFP::TOFU-5 foci (Fig 2D and 2E). We conclude that like its counterpart in *C. elegans*, *C. briggsae* TOFU-5 associates with piRNA-producing genes and likely drives their transcription.

Loss of Piwi causes progressive sterility in *C. briggsae*

Disruption of the piRNA pathway invariably causes sterility of animals examined to date [4, 7, 8, 55, 56]. In *C. elegans*, *prg-1* mutant animals do not become sterile immediately, but rather they become less fertile over generations, a phenotype associated with germ cell mortality [57]. We wondered if loss of *prg-1*/piRNAs in *C. briggsae* renders animals progressively sterile. To this end, we attempted to measure the brood size of wild-type and *Cbr-prg-1* mutant animals. Despite

reported successes [58, 59], we failed to accurately measure the brood size of *C. briggsae* strains because of their burrowing behavior and avoidance to bacterial lawns. To tackle this issue, we decided to assess the fertility in the *Cbr-unc-119* mutant background. The *unc-119* gene encodes a lipid-binding chaperone expressed in the nervous system [60]. *unc-119* mutant animals exhibit slow movement [60], making it easier to measure the brood size. We outcrossed *Cbr-prg-1* with the *Cbr-unc-119* strains, freshly generated the *Cbr-unc-119* and *Cbr-prg-1*; *Cbr-unc-119* double siblings and conducted brood size measurement over generations. The fecundity of the *Cbr-unc-119* strain is maintained over generations. In contrast, *Cbr-prg-1*; *Cbr-unc-119* displayed progressive declines in fertility over generations (Fig 3A).

C. briggsae hermaphrodites produce both sperm and oocytes. To determine whether the infertility of *Cbr-prg-1* mutants results from a defect in oogenesis and/or spermatogenesis, we measured male and female fertility based on four genetic crosses (Fig 3B). When wild-type males mated with unc-119 hermaphrodites, the median brood size was 53 (as measured by counting the total number of non-Unc cross progeny) and 73% hermaphrodites produced non-Unc progeny (Fig 3C). The brood size was decreased when wild-type males were crossed to *Cbr-prg-1* hermaphrodites. Reduction in the brood size was also observed when *Cbr-prg-1* males were crossed to wild-type hermaphrodites (Fig 3C). When *Cbr-prg-1* males mated with *Cbr-prg-1* hermaphrodites, an additive fertility deficit was observed. Only 28% *Cbr-prg-1* hermaphrodites produced non-Unc progeny (Fig 3C). These findings suggest that loss of *prg-1*/piRNAs causes impairment in oogenesis and spermatogenesis.

The Piwi/piRNA pathway is required for germ cell maintenance. For example, loss of Piwi is linked to increased germ cell apoptosis in *C. elegans*, zebrafish and mice [18, 21, 61]. To monitor apoptotic germ cell corpses, we imaged the germ line of late-generation (~40 generation) *Cbr-prg-1* mutants by staining with acridine orange (AO) [62]. AO is capable of entering into corpses

upon increases in membrane permeability and staining DNA [62]. We found apoptotic corpses in gonads of both wild-type and *Cbr-prg-1* mutant strains, but did not observe any statistically significant differences between the two strains (Fig S3A and S3B), indicating loss of *prg-1*/piRNAs does not significantly induce germ cell apoptosis in *C. briggsae.*

C. briggsae piRNAs induce production of 22G-RNAs targeting mRNAs

In *C. elegans*, the PRG-1/piRNAs complex recognizes germline transcripts and recruits RNA-dependent RNA Polymerases (RdRPs) for the production of 22G-RNAs which are loaded onto Worm-specific Argonautes (WAGOs) that maintain and propagate epigenetic silencing [32, 35-39]. *C. briggsae* genome contains at least 10 WAGO genes and 4 RdRP genes (WBGene00038666/*Cbr-rrf-1*, WBGene00024074/*Cbr-rrf-3*, WBGene00023729/*Cbr-ego-1*, and WBGene00026758) [45]. We wondered if *Cbr-PRG-1*/piRNAs induce the production of WAGO 22G-RNAs. Two computational analyses were performed to test this idea. In the first analysis, we predicted piRNA target sites in silico and measured 22G-RNA coverage around putative target sites. 21U-RNA target sites were predicted by mapping *Cbr*-piRNA sequences to the *Cbr*-transcriptome allowing 0 mismatches in the seed region (position 2-8), 1 G:U wobble base-pair in the seed region, 3 mismatches outside the seed region (position 9-21), and 2 G:U wobble base-pairs outside the seed region. This analysis identified 4528 potential piRNA target sites on 3592 gene (1.26 target sites/gene). A 22G-RNA peak directly over the predicted piRNA-binding sites was detected (Fig 4A). In addition, there was a ~1.75-fold enrichment of 22G-RNA levels in wild-type as compared to *Cbr-prg-1* mutants within ±50 nt of predicted piRNA sites. No enrichment was detected in the negative control in which reverse complementary sequences of 21U-RNA sequences were used to predict target sites (Fig 4B). When considering the least abundant (bottom 25%) piRNA species, we found a weak yet noticeable enrichment of 22G-RNAs in wild-type compared to *Cbr-prg-1* animals (Fig 4C). When considering the most abundant (top 25%) piRNA species, we noticed a strong enrichment (2.6-fold) of 22G-RNAs in wild-type relative to the

Cbr-prg-1 animals (Fig 4D). The global analysis was further confirmed by inspecting specific 21U-RNA/target interactions. For example, we observed production of 22G-RNAs that overlapped with or were adjacent to predicted piRNA target sites at WBGene00041650 and WBGene00087786 loci (Fig 4E and 4F).

As for a second analysis, we examined levels of 22G-RNAs targeting individual transcripts. In the *C. elegans* adult germ line, 22G-RNAs can be sorted into distinct pathways including the CSR-1 pathway and WAGO pathway [31, 63]. While *C. briggsae* small RNA pathways require further characterization, one study carefully characterized the Cbr-CSR-1 pathway and defined 4839 genes targeted by Cbr-CSR-1 [64]. When comparing 22G-RNA levels in *cbr-prg-1* mutants to wild-type animals, we found that the Cbr-CSR-1 targets remained largely unchanged (Fig 4G). In contrast, many non-CSR-1 targets, which are resumably targeted by WAGOs, showed depletion of 22G-RNAs in *cbr-prg-1* mutants (Fig 4G). In addition, we identified 1279 predicted 21U-RNA target sites on CSR-1 targets (Fig 4H). Yet no significant enrichment of 22G-RNA levels was detected in wild-type as compared to *Cbr-prg-1*, consistent with the idea that CSR-1 and its small RNAs protect germline mRNAs from piRNA-mediated silencing (Fig 4H) [46, 47]. In total, we defined 858 mRNAs, 3 lincRNAs, 45 pseudogenes, and 4 transposons as Cbr-PRG-1 targets whose 22G-RNAs are significantly depleted upon loss of *prg-1* (Cbr-prg-1/wild-type ≤ 4-fold, p-value < 0.05, reads per million (RPM) ≥ 5 in wild-type, Two-tailed t-test) (Table S2).

Conserved genes are targeted by piRNAs in *C. briggsae* and *C. elegans*

We next assessed the evolutionary conservation of PRG-1 targets between *C. briggsae* and *C. elegans*. ~65% (13179/20157) of *C. briggsae* genes have orthologs in *C. elegans* and ~63% (13179/20997) of *C. elegans* genes have orthologs in *C. briggsae* [64]. We cloned and deep sequenced small RNAs from *C. elegans* wild-type and *prg-1(tm872)* strains and identified 1776 Cel-PRG-1 targets based on the reduction of 22G-RNAs (Cel-prg-1/wild-type ≤ 4-fold, p-value <

0.05, RPM ≥ 5 in wild-type, Two-tailed t-test) (Table S3). When comparing this set with Cbr-PRG-1 targets described above, we found that 58% (526/910) of Cbr-PRG-1 targets had orthologs, a percentage comparable to the genome wide average (Fig 5A). A similar trend was observed in *C. elegans* in which 63% (1120/1776) of Cel-PRG-1 targets possessed orthologs (Fig 5A). We next examined the genomic distribution of PRG-1 targets in *C. briggsae* and *C. elegans*. Cel-PRG-1 targets (n=1776) are relatively uniformly distributed on each chromosome, although they are slightly underrepresented on chromosomes V and X after normalized to number of genes per chromosome. (Fig 5B and S4A). In contrast, Cbr-PRG-1 targets (n=910) are strongly enriched on X chromosome as compared to autosomes (Fig 5C and Fig S4B), suggesting the *C. briggsae* piRNA pathway preferentially targets transcripts expressed from the sex chromosome.

Intriguingly, our analyses identified 88 evolutionarily conserved piRNA targets. These include *xol-1,* a master regulator of X chromosome dosage compensation and sex determination [15, 65] (Table S4). Gene ontology (GO) analysis did not enrich any specific GO terms. Notably, even among conserved piRNA targets, PRG-1-induced 22G-RNA often target different regions of mRNAs. For example, *C. elegans* F43G6.8 (WormBase ID: WBGene00009660) encodes a putative metal ion binding protein. 22G-RNAs target its 5' untranslated region (UTR) as well as the third and fourth exons of the transcript (Fig 5D). In contrast, its *C. briggsae* ortholog, CBG25560 (WormBase ID: WBGene00086974), has abundant 22G-RNAs mapped to its second exons (Fig 5E). 21U-RNAs and their target sites on *C. elegans* F43G6.8 were captured by a method known as crosslinking, ligation, and sequencing of hybrids [33, 66], while 21U-RNAs and their target sites of *C. briggsae* CBG25560 were predicted in silico (see above). In both cases, 22G-RNAs were found to be adjacent to putative piRNA target sites (Fig 5D and 5E). Together, our analyses revealed a set of evolutionarily conserved PRG-1/piRNA targets which are targeted by different piRNAs at different regions.

Loss of piRNAs leads to accumulation of 22G-RNAs at different sets of genes in *C. briggsae* and *C. elegans*

C. elegans piRNA pathway acts to prevent overproduction of 22G-RNAs [40-43]. In particular, upon loss of PRG-1/piRNAs, ribosomal RNAs (rRNAs), histone mRNAs, and additional transcripts are targeted by RdRPs which overamplify 22G-RNAs [40-43]. It has been postulated that mis-regulation of rRNA and/or histone leads to infertility in *C. elegans* [41, 42]. However, it is not clear why a specific set of RNAs are susceptible to 22G-RNA overproduction in *prg-1* mutants.

We reasoned that comparative analysis can offer insights into conserved features of misprocessed RNAs. Consistent with previous findings [40-43], we found 148 genes exhibited elevated 22G-RNA levels in *C. elegans prg-1* mutants (Cel-prg-1/wild-type ≥ 4-fold, RPM ≥ 5 in *prg-1*, p-value < 0.05, Two-tailed t-test). Among them, 69% (102/148) of these genes had orthologs in *C. briggsae* (Fig 6A). Using the same parameters, 96 genes showed upregulated 22G-RNAs in *C. briggsae prg-1* mutants. Among them, 30% (29/96) of genes had orthologs in *C. elegans*, a much lower percentage than the genome-wide average (Fig 6A). To our surprise, zero gene with 1:1 orthologs displayed elevated 22G-RNAs in *C. elegans* and *C. briggsae* (Fig 6A).

We examined 22G-RNAs that specifically target rRNAs and histone mRNAs. In *C. elegans*, levels of 22G-RNAs that are mapped to 39 histone loci were significantly elevated in *prg-1* mutants (Fig 6B) [40, 41, 43]. And the median abundance of 22G-RNAs was upregulated 6.7-fold in *prg-1* mutants as compared to wild-type (Fig 6B). In *C. briggsae*, however, most of histones did not display increased 22G-RNAs when *prg-1* is mutated (Fig 6C). In *C. elegans*, 22G-RNAs from rrn-1.1, rrn-2.1 and rrn-3.1 were aberrantly accumulated in *prg-1* mutants (Fig 6B) [42, 43]. Specifically, the median abundance of 22G-RNAs in *prg-1* was increased 5.5-fold relative to wild-type (Fig 6B). In contrast, the level of 22G-RNA produced from rRNAs remained largely unchanged in *C. briggsae prg-1* mutant animals as compared to wild-type (Fig 6C). Together, our

analyses revealed that a unique set of RNAs accumulate 22G-RNAs in *C. briggsae* and *C. elegans* upon loss of *prg-1*.

Relationship between splicing and hyper-accumulation of 22G-RNAs

We carried out comparative analysis to investigate common features of RNAs that are prone to 22G-RNA overamplification in the absence of piRNAs. 5' UTR and 3' UTR were examined due to their important regulatory functions [67, 68]. We compared transcripts exhibiting upregulated 22G-RNA levels to the control groups which are germline-expressed transcripts whose 22G-RNAs levels did not alter in *prg-1* mutants. No clear trend was detected regarding lengths of 5' UTR and 3' UTR in *C. briggsae* and *C. elegans* (Fig S5A-D). For example, 5' UTR of RNAs (n = 148) with elevated 22G-RNAs are longer than the control group in *C. elegans*, while 5' UTR of genes (n = 96) with elevated 22G-RNAs are shorter than the control set in *C. briggsae* (Fig S5A and S5C). The length of 3' UTR in *C. elegans* and *C. briggsae* displayed an opposite trend (Fig S5B and S5D). Next, we examined introns, as there is evidence for the intimate interplay between pre-mRNA splicing and small RNA biogenesis [69-72]. We noticed that transcripts with upregulated 22G-RNA levels possess fewer introns in both *C. elegans* and *C. briggsae* relative to control groups which are germline-expressed transcripts whose 22G-RNAs levels did not upon loss of *prg-1* (Fig 6D and 6E), indicating abundant introns or pre-mRNA splicing events may inhibit RdRP-mediated 22G-RNA production. Indeed, when further grouping *C. elegans* histone genes into intron-containing histones and intronless histones, we found that intronless histone group, but not the intron-containing histones, exhibited increased 22G-RNAs in *prg-1* mutants relative to wild-type (Fig S5E).

To directly test the causal relationship between splicing and 22G-RNA synthesis, we assessed 22G-RNAs produced from the endogenous *C. elegans oma-1* gene and an intronless *oma-1* allele in which all intronic sequences were removed [72]. In strains expressing wild-type (intron-

containing) *oma-1*, small RNA sequencing revealed comparable levels of 22G-RNAs between *wild-type* and *prg-1* mutants (Fig 6F). 22G-RNAs were primarily mapped to exons, suggesting RdRPs use spliced *oma-1* mRNA as template to synthesize 22G-RNAs (Fig 6F). In wild-type and *prg-1* mutant strains expressing intronless *oma-1*, abundant 22G were detected. In particular, loss of *prg-1* led to at least 5-fold increase in 22G-RNA level when compared to wild-type (Fig 6G) [72]. Altogether our findings suggest the presence of functional introns—likely splicing itself or deposition of exon junction complex—prevents 22G-RNA overproduction in *prg-1* mutants (see Discussion below).

DISCUSSION

In this study, we defined piRNA-producing loci and characterized piRNA functions in *C. briggsae*, a sibling species that separated from *C. elegans* about 100 million years ago [44]. Our comparative studies uncovered both conserved and species-specific features in the nematode piRNA pathways. Specifically, we identified over 25,000 C. *briggsae* piRNAs, a number that is comparable to that of their counterparts in *C. elegans* [18-21]. Although the architecture of piRNA genes and chromatin factors associated with piRNA clusters appeared to be conserved, piRNA/21U-RNA sequences have diverged rapidly (Fig 1 and 2). Thus, piRNA sequences themselves are under little selective pressure. In contrast, the biogenesis mechanism and the number of piRNAs are under strong selection. How are over 20,000 piRNAs-producing genes maintained over 100 million years of evolution? And how do new piRNA genes arise? In flies, new piRNA species are produced when invading transposons are inserted into piRNA clusters and dispersed genomic regions [73, 74]. In worms, however, transposons are not enriched at piRNA clusters, nor did the majority of piRNAs display sequence complementarity to transposons. Thus, a yet undiscovered mechanism may be responsible for the generation of new piRNA-producing genes.

One interesting function of *C. elegans* piRNAs appears to be the recognition and silencing of newly introduced foreign sequences [35-38]. For example, piRNAs initiate epigenetic silencing on transgenes that express the jellyfish green fluorescent protein (*gfp)*, even though piRNAs do not perfectly match *gfp* sequence [37]. By allowing mismatches between piRNAs and their target RNAs, PRG-1 can recognize the target and recruit RdRPs to initiate the biogenesis of 22G-RNAs [35-39]. Our analysis revealed that *C. briggsae* piRNA pathway induces WAGO 22G-RNAs from hundreds of germline transcripts (Fig 3A). While CSR-1/22G-RNAs targets are highly conserved in *C. elegans* and *C. briggsae* [64], PRG-1/piRNA targets have diverged rapidly (Fig 5). Nevertheless, 88 orthologous genes were found to be targeted by both *C. briggsae* and *C. elegans* piRNA pathways (Table S4). We envision that regulation of these evolutionarily conserved piRNA targets may promote fertility or contribute to other important physiological processes. Indeed, *xol-1*, one of the piRNA targets, is linked to worm dosage compensation and sexual development [15, 65]. Additional genetic and biochemical experiments will be required to determine physiological roles of other conserved piRNA targets.

Previous studies and our work here showed that *C. elegans* and *C. briggsae* piRNA pathways prevents overamplification of 22G-RNAs (Fig 6) [40-43]. In both organisms, RNAs with fewer introns are more susceptible for 22G-RNA overproduction. Removal of introns from *oma-1*, an endogenous gene, led to increased 22G-RNA levels when *prg-1* is mutated (Fig 6G). These findings suggest that introns and/or efficient pre-mRNA splicing limits 22G-RNA overamplification. A connection between splicing and small RNA synthesis has been first demonstrated in yeast *Cryptococcus neoformans* and later found in nematode *C. elegans*, where stalled or inefficient splicing direct transcripts into the RNA interference (RNAi) pathway [70, 72, 75]. It is thought that some RNAi components surveil splicing to detect invasive sequences such as transposons and viral genomes. We envision that loss of *prg-1* frees up some RdRPs and WAGOs. It is possible that RdRPs intrinsically favor intronless and/or poorly spliced transcripts as templates to

synthesize 22G-RNAs. Presumably, RNAs with fewer introns have fewer exon-junction complexes (EJCs). EJC are deposited onto RNAs during splicing, and plays key roles in their export, localization, and turnover [76]. A highly speculative hypothesis predicts EJC physically blocks the 3' to 5' polymerase activity of RdRPs. Alternatively, EJC may prevent RNAs from entering into mutator foci where 22G-RNAs are synthesized [77]. It is not clear why intronless histone mRNAs are immune to 22G-RNA overamplification in *prg-1 C. briggsae*. Previous studies reported a positive feedback loop in which 22G-RNAs initiate cleavage followed by pUGylation of RNAs and RdRPs use pUGylated RNAs as templates to synthesize more 22G-RNAs [78]. We noticed some basal levels of 22G-RNA in wild-type *C. elegans*, while 22G-RNAs targeting histone mRNAs are absent in wild-type *C. briggsae*. Perhaps *C. elegans* histone mRNAs, but not *C. briggsae* counterparts are primed for 22G-RNA overamplification. The presence of 22G-RNAs and/or pUGylated RNAs may be required for triggering 22G-RNA overproduction upon loss of *prg-1*/piRNAs.

Finally, significant progress has been made in understanding piRNA biogenesis and function using model systems including *D. melanogaster*, *C. elegans* and mouse [1-3]. However, studies should not be limited to model organisms. In the past, next-generation sequencing technology has been employed to define piRNAs in non-model organisms [79-81]. With the advent of CRISPR genome editing tools [82], one can start interrogating piRNA targets and functions in non-model organisms. Comparative genomic and functional studies will be essential to understand the rapidly evolving piRNA pathway.

MATERIALS AND METHODS

Worm strains

AF16 and N2 strain are reference strains for *C. briggsae* and *C. elegans* respectively. Worms were cultured according to standard methods at 20 °C unless otherwise indicated [83]. Mutant animals were generated using CRISPR editing or obtained from the CGC. To generate *C. briggsae* transmission lines expressing an extrachromosomal piRNA array, a DNA fragment on chromosome IV was amplified by PCR and cloned into the Topo vector (Thermofisher). Plasmids were purified by miniprep and injected to WHY341 (*GFP::FLAG::AID::Cbr-tofu-5 I; Cbr-unc-119(nm67) III*) with co-injection marker pCFJ151 in a 3:1 ratio [84]. Transmission lines were established by single-picking non-unc F1 and subsequently non-unc F2. All strains used in this study are listed in Table S5.

CRISPR genome editing

CRISPR/Cas9-generated strains were made as previously described [85]. In brief, double-stranded donor (500 ng) or single-stranded donor (2.2 µg) was used to introduce GFP:AID:FLAG to *tofu-5* or 3xFLAG to *prg-1*, respectively. Repair template donors were added to pre-assembled Cas9 ribonucleoprotein complex (5 µg Cas9, 2 µg gRNA, 1 µg tracrRNA) (IDT). Plasmid pRF4::rol-6(su1006) was used as a co-injection marker [85].

Total RNA isolation

Approximately 100,000 synchronized L1 animals were plated on 135 mm NGM plates seeded with OP50 and grown at 20 °C until the animals reached gravid adult stage. Gravid adult populations were harvested using M9, and subsequently suspended in Trizol. Worms were lysed using the Fisherbrand Bead Mill 24 homogenizer, bromochloropropane was added to the lysis to perform RNA extraction. Isopropanol was then used to precipitate RNA from the aqueous phase.

Small RNAs were isolated from total RNAs using the miRVana miRNA isolation kit (Thermo Fisher Scientific) according to the manufacturers protocol.

Small RNA sequencing

Small RNA samples from wild-type and mutants were first incubated with a recombinant 5' polyphosphatase PIR-1 which removes the γ and β phosphates from 5´-triphosphorylated RNAs [48, 86]. The resulting monophosphorylated RNAs were ligated to the 3' adaptor (5'rAppAGATCGGAAGAGCACACGTCTGAACTCCAGTCA/3ddC/3', IDT) using T4 RNA ligase 2 in the presence of 25% PEG8000 (NEB) at 15 °C overnight. The 5' adaptor (rArCrArCrUrCrUrUrUrCrCrCrUrArCrArCrGrArCrGrCrUrCrUrUrCrCrGrArUrCrU, IDT) was then ligated to the product using T4 RNA ligase 1 (NEB) at 15 °C for 4 hours. The ligated products were converted to cDNA using SuperScript IV Reverse Transcriptase (Thermo Fisher Scientific). The cDNAs were amplified by PCR using Q5 High-Fidelity DNA polymerase (NEB), and the libraries were sequenced on an Illumina Novaseq platform (SP 2 X 50 bp) at the OSU Comprehensive Cancer Center genomics core.

Fluorescence microscopy

Live worms suspended in 1x M9 buffer were immobilized with 0.2 mM tetramisole (Sigma-Aldrich) and mounted on fresh 1% agar pads. Airyscan images were acquired using a Zeiss Axio Observer microscope equipped with an Airyscan 2 detector and a 40x water objective. Image processing was performed using standard 3D Airyscan processing.

Germline apoptosis and scoring

To quantify germline apoptosis, synchronized *C. briggsae* wild-type and *prg-1* mutant worms plated on Day 1 were grown at 20°C until Day 4. On Day 4, 50 worms per experiment were transferred to a fresh plate. 200 µL Acridine Orange (AO) stain (75 µg/mL in M9) was distributed

evenly to the fresh plates and allowed to dry in the dark. After feeding on the AO-soaked bacterial lawn in the dark at 20°C for 1 hour, the worms were transferred to a clean plate seeded with *E. coli* and incubated in the dark for 2 hours to clear excess dye from the intestines. The worms were imaged under the 40x objective with fluorescence microscopy to quantify the number of apoptotic corpses per gonad arm. One gonad arm was scored per animal, and 33-40 animals scored per experiment.

Multigenerational Brood Size Assays

C. briggsae wild-type (AF16) and *prg-1* mutant brood sizes were assayed at 25°C in an *unc-119(nm67)* background. After outcross, 25 independent lines for each strain were continuously grown each generation by transferring 4 L4 larvae per line to new plates. Brood Size assays were performed approximately every two generations. To assay brood size, 1 L4 larvae per line was placed singly on plates. The animals were transferred halfway through egg-laying and the total brood size for each animal was calculated by adding the progeny of the original and transferred plates.

Mating assays

To test mother-dependent and/or father-dependent fertility defects of *C. briggsae prg-1* mutants, male stocks of *C. briggsae* wild-type AF16 or *prg-1* mutants were generated via self-cross. For each cross, 5 *unc-119(nm67)* hermaphrodites were plated with 10 males, with a total of 29-60 hermaphrodites per experiment. Animals were allowed to cross overnight at 20°C and single picked to new plates the next day. The mothers were transferred mid-egg laying and the total wild-type looking (non-Uncoordinated) cross progeny for each animal was calculated by adding the wild-type cross progeny from the original and transferred plates. Animals with no wild type looking progeny, either from unsuccessful crosses or fertility defects, were recorded as zero.

Small RNA sequencing data analysis

Raw small RNA sequencing reads were parsed from adapters and low-quality reads using TrimGalore and assessed using FastQC. 15-40 nucleotide long reads were collapsed using custom shell scripts and aligned to the C. *elegans* or C. *briggsae* (WormBase release WS279) genome reference using Bowtie with the parameters -v 0 -m 1 -a --best --strata to obtain perfectly and uniquely mapped smRNA sequencing alignments [87]. Due to the repetitive nature of histone and rRNA genes, we realigned our smRNA sequencing reads to the genome using the Bowtie parameters -v 0 -m 1000 -a --best --strata to capture multimapping reads associated with these features [87]. Reads failing to align to the genome reference were realigned to a reference containing exon-exon junctions using the same Bowtie parameters. Exon-exon junction mapping reads were converted to genomic coordinates using custom python scripts and added to the genomic alignment. Sam alignment files were then converted to bed files using BEDOPS [88]. Following alignment, reads were normalized to the number of times mapped, and assigned to genomic features using BEDtools and custom python scripts [89]. Briefly, reads were filtered based on first nucleotide, length, strand orientation, 5' to 5' distance between read and feature using the following parameters: 1) *piRNAs.* Reads must map sense to piRNA loci, contain a 5' U, 20-33 nt long and align to position 0,1 or 2 of annotated 5' piRNA end; 2) *22G-RNAs.* Reads must map antisense to protein coding gene exon, pseudogene exon, lincRNA, rRNA, or annotated transposon. Only reads 21-23 nt in length starting with a 5' G were considered.

Reads assigned to multiple genomic features were further processed using a hierarchical based filtering approach. Briefly, reads mapping to highly contaminating RNA species such as ncRNA, tRNA, snRNA, snoRNA, and rRNA were given priority over other features. Read counts for other multi-feature mapping reads were split equally amongst the number of features mapped. In addition to genome mapping reads were mapped to RepBase transposon consensus sequences and filtered using the same parameters described above [90]. Of note, rRNAs are poorly annotated in the C. *briggsae* reference genome, thus, smRNA sequencing reads from C. *briggsae*

wild-type and *prg-1* mutants were aligned to the C. *elegans* reference to quantify 22G-RNAs targeting rRNAs.

Defining *C. briggsae* piRNA-producing genes

Reads from IP and input samples were processed using TrimGalore and assessed using FastQC. Processed reads 15-40 nt in length were collapsed using custom shell scripts and aligned to the C. *briggsae* genome reference (WS279) using the Bowtie with the parameters -v 0 -m 1 [87]. Sam alignments were converted to bed files using BEDOPS [88]. Following alignment, IP reads with a count of less than 2 were removed. Aligned reads passing filters were then grouped based on their strand and 5' nucleotide position. For a given genomic position/strand group reads were collapsed into unique loci; the length of the locus was determined as the length of the most abundant read within each group. Collapsed loci were then compared between IP and input samples by calculating fold change using the formula $\frac{IP + 0.01}{input + 0.01}$, for both replicates of IP, as well as derivation of p-values using a Two-tailed t-test. Enriched loci were defined by 4-fold enrichment in both IP samples, and a p-value of less than 0.05. The 5' nucleotide and length of enriched loci were plotted to elucidate the length and 5' preference of C. *briggsae* piRNAs. Following this analysis, loci that are 21-nt in length starting with 5' U were considered as C. *briggsae* piRNA.

Motif Analysis

Genomic sequences 60 nts up and down stream of piRNA 5' ends were isolated using BEDtools [89]. MEME motif analysis software was then used to construct sequence logos [91].

21U-RNA target site prediction

21U-RNA target sites were predicted using an analysis approach similar to that described [92]. Briefly, 21U-RNA sequences were aligned to a transcriptome reference containing protein coding

genes, pseudogenes, lincRNAs and RepBase transposon sequences allowing up to 6 mismatches with BWA [90, 93]. Aligned sequences were then further processed to annotate the number of seed mismatches, seed G:U base-pairs, non-seed mismatches, non-seed G:U base-pairs, of each piRNA-target interaction using custom python scripts. For downstream metagene analysis piRNA target sites with less than or equal to 1 seed G:U bp, 3 non-seed mismatches, and 2 non-seed GU bp were considered.

Density of 22G-RNAs

Processed collapsed smRNA reads were aligned to the same transcriptome reference used in 21U-RNA target site prediction using Bowtie. Sam files were converted to bedfiles using BEDOPS [88]. Antisense mapping 21-23 nt reads starting with G were then filtered from bed files. The per-base 22G-RNA coverage, normalized to total genome matching reads, was then calculated for all transcripts using custom python scripts. Regions of transcripts within 120 nucleotides of a piRNA target site were isolated and aggregated based on the relative position to the 10th nucleotide of the piRNA. Plots showing the coverage of 22G-RNAs are of two averaged biological replicates and were drawn in R. piRNA target sites were assigned to genomic coordinates by mapping the target sequence to the genome using Bowtie.

Definition of intronless and intron-containing histone genes

Histone genes were grouped into two categories based on the presence or absence of introns according to WormBase (WS279) annotation. Although *his-57* is annotated to have three isoforms (one is intronless and the other two contains introns), 22G-RNAs are found to be produced exclusively from the intronless isoform. Thus we reasoned that his-57 is likely mis-annotated and considered it as an intronless histone gene.

Quantification and Statistical Analyses

All statistical tests used in this study are listed in the figure legends. Statistical tests and plots were preformed using custom R scripts. The major R packages used in the analysis of the data were dplyr, ggplot2, and other packages from Tidyverse [94].

DATA AVAILABILITY

The *C. briggsae* PRG-1 IP, as well as small RNA sequencing data from wild type and *prg-1* mutant *C. elegans* and *C. briggsae* strains are available at GEO under the accession number GSE203297 (https://www.ncbi.nlm.nih.gov/geo/query/acc.cgi?acc=GSE203297 with secure token: gjyxmswqnxgzxsb). CSR-1 IP data are available at NCBI SRA under the accession number SRP021463 [64]. CLASH sequencing data used in this study to define piRNA target sites are available at NCBI SRA under the accession number SRP131397 [33].

ACKNOWLEDGMENTS

We thank D. Schoenberg for discussion and comments; S. Tu for assistance in initial data analysis; the Neuroscience Imaging Core for instruments (S10OD026842); the OSU Comprehensive Cancer Center genomics core for Illumina sequencing. Some of the *C. elegans* and *C. briggsae* strains were provided by the Caenorhabditis Genetics Center supported by National Institutes of Health (P40 OD010440). This work was supported by National Institutes of Health Pathway to Independence Award (R00GM124460) and Maximizing Investigators' Research Award (R35GM142580) to W.T.

CONFLICT OF INTEREST

The authors declare that there is no competing interest.

FIGURES LEGENDS

Figure 1: Identification and Characterization of piRNA-producing loci in *C. briggsae.*

(A) Scatter plot showing the normalized abundance of sequence reads in 3XFLAG::Cbr-PRG-1 IP and Input samples. Data are displayed as an average of two biological replicates. Green dots mark reads 4-fold enriched in IP samples with a two-tailed t-test p-value < 0.05. Dotted grey diagonal lines represent 4-fold enrichment, no change in abundance, and 4-fold depletion, respectively.

(B) Barplot showing the length and first nucleotide distribution of enriched reads from 3XFLAG::Cbr-PRG-1. Data are displayed as the fraction of enriched reads based on RPM from two averaged 3XFLAG::Cbr-PRG-1 IP biological replicates.

(C) Barplot showing the overall abundance of C. *briggsae* piRNAs as determined by small RNA sequencing in wild-type and *prg-1* mutant animals. The error bars represent the mean ± the standard deviation of two biological replicates. A Two-tailed t-test was used to derive p-values.

(D) Heatmap showing the percentages of C. *briggsae* piRNAs, miRNAs, and tRNAs mapping to a reference of *C.* elegans piRNAs, miRNAs, and tRNAs with 0, 1, 2, or 3 mismatches, respectively.

(E) Barplots showing the location and abundance of piRNAs on each chromosome in C. *briggsae*. Blue bars represent piRNA loci residing on the forward strand of DNA, red bars represent loci residing on the reverse strand. The height of the bar reflects the abundance of each loci as an average of two PRG-1 IP biological replicates. 302 piRNA genes are mapped to contigs that do not have genomic coordinates and therefore are not presented in this panel.

(F) Bits plots showing the nucleotide preference within a 60-nucleotide window up and down stream of annotated piRNA genes that reside within and outside of piRNA clusters on chromosomes I and IV.

Figure 2: *C. briggsae* TOFU-5 associates with piRNA clusters.

(A) Schematic of germline zones (mitotic or meiotic) imaged to assess GFP:TOFU-5 localization.

(B-C) Maximum intensity projections of a z stack spanning mitotic (left) and meiotic (right) germline nuclei of live *C.elegans* worms expressing Cel-GFP::TOFU-5 (40x objective) (B) and *C. briggsae* worms expressing Cbr-GFP::TOFU-5 (40x objective) (C). Dashed lines outline the position of germ nuclei. Scale bar = 5 μm.

(D) Maximum intensity projections of a z stack spanning germline nuclei of live *C. briggsae* worms expressing GFP::TOFU-5 with extrachromosomal arrays expressing piRNA genes in the mitotic (left) and meiotic (right) zone (40x objective). Dashed lines outline the position of wild-type germ nuclei (white) and germ nuclei presumably containing piRNA arrays (red). Scale bar = 5 μm.

(E) Quantification of GFP::TOFU-5 foci in live *C. elegans* (B), *C. briggsae* (C), and *C. briggsae* with extrachromosomal piRNA arrays (D). The violin plot shows the number of foci per nuclei for three biologically independent experiments, with at least 40 nuclei quantified in the mitotic (*Cel* n=40; *Cbr* n=48; *Cbr* + piRNA array n=45) and meiotic (*Cel* n=57; *Cbr* n=45; *Cbr* + piRNA array n=46) zone. Statistically significant differences were determined using a Two-tailed Wilcoxon Rank Sum Test (*p<0.05, ****p < 0.0001).

Figure 3: Loss of Piwi causes progressive sterility in *C. briggsae.*

(A) Multigenerational brood size assay of *C. briggsae unc-119(nm67)* (blue and serves as wild-type control) and *prg-1; unc-119* (red) mutant animals at 25°C. The boxplots show the median (center line), 25 and 75th percentile (box edges), and the whiskers indicate the median +/- 1.5 x interquartile range. Fertility was assayed the following generations after outcross: 1 (wild-type n=15; *prg-1* n=15), 2 (wild-type n=17; *prg-1* n=19), 3 (wild-type n=22; *prg-1* n=25), 5 (wild-type n=22; *prg-1* n=25), 7 (wild-type n=23; *prg-1* n=24), 9 (wild-type n=21; *prg-1* n=21), and 14 (wild-type n=25; *prg-1* n=25). A Two-tailed Wilcoxon Rank Sum Test was used to compare fecundity of wild-type and *prg-1* mutants at each generation (ns = no significance, *p<0.05, **p<0.01, ***p<0.001, ****p < 0.0001).

(B) Schematic of the cross strategy. *unc-119* mutant mothers were crossed with wild-type AF16 (cross 1) or *prg-1* mutant (cross 3) males. *prg-1*; *unc-119* mutant mothers were crossed to wild-type AF16 (cross 2) or *prg-1* mutant (cross 4) males. *prg-1* mutants are indicated by red.

(C) Mating assay showing the median number of non-Uncoordinated (non-Unc) cross-progeny for each cross (cross 1, n=30; cross 2, n=30; cross 3, n=28; cross 4, n=60). The percentage of crosses with no non-Unc cross-progeny are shown. A Two-tailed Wilcoxon Rank Sum Test was used to compare total non-Unc cross-progeny, with the following significance indicators: (ns = no significance, *p<0.05, **p<0.01, ***p<0.001, ****p < 0.0001).

Figure 4: *C. briggsae* piRNAs induce production of 22G-RNAs mapped to endogenous mRNAs.

(A-D). Line plots showing the coverage of 22G-RNAs within a 110 nt window centered on the 10th nucleotide of targeting piRNAs for all predicted target sites (A), all predicted target sites using reverse complementary 21U-RNAs (B), target sites for the 25% least/most abundant piRNAs by IP RPM (C and D). Blue lines represent the coverage in wild-type and red lines indicate the

coverage in *prg-1* mutants. Data are displayed as an average of two biological replicates, shaded regions indicate the standard deviation at each position plotted. Above each plot are the total number of piRNA target sites and the number of target sites per gene.

(E-F) Browser view of 22G-RNA signal at predicted piRNA target sites on WBGene00041650 (E) and WBGene00087786 (F). Coverage of 22G RNAs along the transcript are shown for wild-type (blue) and *prg-1* mutants (red). A red bar within the gene model marks the precise 21UR-3346 and 21UR-3955 (E) and 21UR-452 (F) target sites. Above each red bar is a schematic illustrating the predicted base-pairing pattern between piRNAs and targets. Mismatched base-pairs are shown in red and G:U base-pairs are shown in green along with a + sign.

(G) Scatter plot showing the abundance of 22G-RNAs targeting protein-coding genes, pseudogenes, lincRNAs, and transposons in *prg-1* and wild-type *C. briggsae*. Purple dots indicate CSR-1 targets annotated in [64]. Turquoise dots represent transcripts that are 4-fold depleted of 22G-RNAs (Two-tailed t-test, p-value < 0.05).

(H) Line plot of the 22G-RNA levels within a 110 nt widow centered on the 10th nucleotide of piRNAs on CSR-1 targets is shown. Data are displayed as an average of two biological replicates, shading above each line represent the standard deviation between the two biological replicates at each point. The number of target sites as well as the number of sites per gene are indicated above the plot.

Figure 5: PRG-1 targets in *C. briggsae* and *C. elegans*.

(A) Venn diagram showing the overlap of orthologous genes with decreased 22G-RNA abundance in C. *elegans* and C. *briggsae prg-1* mutants. The breakdown of non-overlapping genes with / without orthologs in the other species is shown as pie charts within each circle.

(B-C) Barplots showing the number of PRG-1 targets per total number of genes per chromosome in *C. elegans* (B), and *C. briggsae* (C).

(D and E) Genome browser view of 22G RNA coverage near piRNA target sites for a conserved orthologous PRG-1 target pair: *C. elegans* transcript F43G6.8 (D), and the *C. briggsae* transcript CBG25560 (E). In each gene model red bars denote the location of putative piRNA target sites. *C. elegans* piRNA target sites were defined using *C. elegans* PRG-1 CLASH data [33]. *C. briggsae* piRNA target sites were predicted based on prediction (See Materials and Methods).

Figure 6: Characterization of genes that accumulate 22G RNAs in *prg-1* mutants.

(A) Venn diagram showing the overlap of orthologous genes with increased 22G-RNA levels in C. *elegans* and C. *briggsae prg-1* mutants. The breakdown of non-overlapping genes with / without orthologs in the other species is shown as pie charts within each circle.

(B-C) Boxplots showing the abundance of 22G-RNAs targeting histone genes and ribosomal RNAs in *C. elegans* (B) and *C. briggsae* (C). p-values were derived using a Two-tailed t-test.

(D-E) Boxplots showing the number of introns in genes with accumulated 22G RNAs in *C. elegans* (D) and *C. briggsae* (E) *prg-1* mutants. The sample size of control and genes with upregulated 22G RNAs in *C. elegans* and *C. briggsae* are denoted in x-axis labels. Genes in the control set are expressed in the germ line and do not exhibit changes in 22G-RNA levels in *prg-1* mutants. p-values were derived using a Two-tailed Wilcoxon Rank Sum Test.

(F-G) Histograms represent the position and abundance of 5' end of 22G-RNAs targeting *C. elegans oma-1* transcript (F) or intronless *C. elegans oma-1::3xflag* (G) [72]. Blue bars represent reads from wild-type samples; red bars indicate reads from *prg-1* mutant samples.

Figure S1. Expression of 3xFLAG::PRG-1 and piRNAs.

(A) Western blotting analysis of 3xFLAG::PRG-1 in wild-type *C. briggsae* and *C. briggsae* expressing 3 x FLAG::PRG-1 with anti-FLAG antibody (top) and anti-Tubulin antibody (bottom). The asterisk denotes a background band.

(B-C) Genome browser view of discrete and overlapping C. *briggsae* piRNA-producing loci. The scale of Cbr-PRG-1 IP (blue) and input (red) was adjusted so that reads from individual samples could be visualized.

(D) Boxplot displaying the abundance of Type I (within clusters) and Type II (outside clusters) piRNA in C. *briggsae* as determined by small RNA sequencing. The thick bar within each box represents the median normalized piRNA abundance in each category. A Two-tailed Wilcoxon Rank-Sum test was used to derive p-values.

Figure S2: Sequence alignment between Cel-TOFU-5 and Cbr-TOFU-5.

The alignment shows *C. elegans* and *C. briggsae* TOFU-5 protein sequences and their putative SANT domains.

Figure S3: Acridine Orange staining of apoptotic corpses in the *C. briggsae* germline.

(A) Representative brightfield and GFP fluorescence images of Acridine Orange (AO) stained germ lines of live adult wild-type and *prg-1* mutant animals under a 40x objective for the detection of germ cell apoptosis. Dashed lines outline the position of germline. Scale bar = 20 μm.

(B) Bar plots quantifying the mean number of Acridine Orange (AO)-positive germ cells per gonad arm. in wild-type (blue, n=40) and *prg-1* mutant (red, n=33) animals. Each point represents a gonad arm assayed per animal. The Two-tailed Wilcoxon Rank Sum Test was used to compare number of AO corpses, ns represents p-value ≥ 0.05.

Figure S4: Genomic location of PRG-1 targets in *C. elegans* and *C. briggsae*.

(A-B) Karyotype style plots showing the gene density (grey bars) as well as location of PRG-1 targets (red bars) along chromosomes I-X in *C. elegans* (A) and *C. briggsae* (B).

Figure S5: Length of 5' and 3' UTRs in *C. elegans* and *C. briggsae* for genes that accumulate 22G RNAs in *prg-1* mutants.

(A-D) Boxplots showing the length of 5' UTR (A and C) and 3' UTR (B and D) in *C. elegans* (A and B) and *C. briggsae* (C and D) for transcripts that accumulate 22G-RNAs in *prg-1* mutants. The sample size of control and genes with upregulated 22G-RNAs in *C. elegans* and *C. briggsae* are denoted in x-axis labels. Genes in the control set are expressed in germline and do not exhibit changes in 22G-RNA levels in *prg-1* mutants. p-values were derived using a Two-tailed Wilcoxon Rank Sum Test.

(E) Boxplot showing the abundance of 22G-RNAs targeting intronless or intron-containing histone genes in wild-type and *prg-1* mutant animals. P-values were derived using a Two-tailed t-test.

Supporting Information

Table S1. *C. briggsae* piRNA genes defined by the enrichment from Cbr-PRG-1 IP.

Table S2: 22G-RNA density in *C. briggsae.*

Table S3: 22G-RNA density in *C. elegans.*

Table S4: Conserved PRG-1 Targets in *C. briggsae* and *C. elegans.*

Table S5: Worm strains used in this study.

REFERENCES

1. Ozata DM, Gainetdinov I, Zoch A, O'Carroll D, Zamore PD. PIWI-interacting RNAs: small RNAs with big functions. Nature reviews Genetics. 2019;20(2):89-108. Epub 2018/11/18. doi: 10.1038/s41576-018-0073-3. PubMed PMID: 30446728.
2. Weick EM, Miska EA. piRNAs: from biogenesis to function. Development. 2014;141(18):3458-71. doi: 10.1242/dev.094037. PubMed PMID: 25183868.
3. Luteijn MJ, Ketting RF. PIWI-interacting RNAs: from generation to transgenerational epigenetics. Nat Rev Genet. 2013;14(8):523-34. Epub 2013/06/26. doi: 10.1038/nrg3495. PubMed PMID: 23797853.
4. Cox DN, Chao A, Baker J, Chang L, Qiao D, Lin H. A novel class of evolutionarily conserved genes defined by piwi are essential for stem cell self-renewal. Genes Dev. 1998;12(23):3715-27.
5. Aravin AA, Hannon GJ, Brennecke J. The Piwi-piRNA pathway provides an adaptive defense in the transposon arms race. Science. 2007;318(5851):761-4. Epub 2007/11/03. doi: 10.1126/science.1146484. PubMed PMID: 17975059.
6. Lin H, Spradling AC. A novel group of pumilio mutations affects the asymmetric division of germline stem cells in the Drosophila ovary. Development. 1997;124(12):2463-76.
7. Houwing S, Kamminga LM, Berezikov E, Cronembold D, Girard A, van den Elst H, et al. A role for Piwi and piRNAs in germ cell maintenance and transposon silencing in Zebrafish. Cell. 2007;129(1):69-82. Epub 2007/04/10. doi: 10.1016/j.cell.2007.03.026. PubMed PMID: 17418787.
8. Carmell MA, Girard A, van de Kant HJ, Bourc'his D, Bestor TH, de Rooij DG, et al. MIWI2 is essential for spermatogenesis and repression of transposons in the mouse male germline. Developmental cell. 2007;12(4):503-14. doi: 10.1016/j.devcel.2007.03.001. PubMed PMID: 17395546.
9. Malone CD, Hannon GJ. Small RNAs as guardians of the genome. Cell. 2009;136(4):656-68. doi: 10.1016/j.cell.2009.01.045. PubMed PMID: 19239887; PubMed Central PMCID: PMC2792755.
10. Senti KA, Brennecke J. The piRNA pathway: a fly's perspective on the guardian of the genome. Trends in genetics : TIG. 2010;26(12):499-509. doi: 10.1016/j.tig.2010.08.007. PubMed PMID: 20934772.
11. Siomi MC, Sato K, Pezic D, Aravin AA. PIWI-interacting small RNAs: the vanguard of genome defence. Nature reviews Molecular cell biology. 2011;12(4):246-58. doi: 10.1038/nrm3089. PubMed PMID: 21427766.
12. Dai P, Wang X, Gou LT, Li ZT, Wen Z, Chen ZG, et al. A Translation-Activating Function of MIWI/piRNA during Mouse Spermiogenesis. Cell. 2019;179(7):1566-81 e16. Epub 2019/12/14. doi: 10.1016/j.cell.2019.11.022. PubMed PMID: 31835033; PubMed Central PMCID: PMCPMC8139323.
13. Wu PH, Fu Y, Cecchini K, Ozata DM, Arif A, Yu T, et al. The evolutionarily conserved piRNA-producing locus pi6 is required for male mouse fertility. Nat Genet. 2020;52(7):728-39. Epub 2020/07/01. doi: 10.1038/s41588-020-0657-7. PubMed PMID: 32601478; PubMed Central PMCID: PMCPMC7383350.
14. Kiuchi T, Koga H, Kawamoto M, Shoji K, Sakai H, Arai Y, et al. A single female-specific piRNA is the primary determiner of sex in the silkworm. Nature. 2014;509(7502):633-6. doi: 10.1038/nature13315. PubMed PMID: 24828047.

15. Tang W, Seth M, Tu S, Shen EZ, Li Q, Shirayama M, et al. A Sex Chromosome piRNA Promotes Robust Dosage Compensation and Sex Determination in C. elegans. Dev Cell. 2018;44(6):762-70 e3. Epub 2018/02/20. doi: 10.1016/j.devcel.2018.01.025. PubMed PMID: 29456136; PubMed Central PMCID: PMCPMC5991626.
16. Ross RJ, Weiner MM, Lin H. PIWI proteins and PIWI-interacting RNAs in the soma. Nature. 2014;505(7483):353-9. doi: 10.1038/nature12987. PubMed PMID: 24429634.
17. Fang W, Wang X, Bracht JR, Nowacki M, Landweber LF. Piwi-interacting RNAs protect DNA against loss during Oxytricha genome rearrangement. Cell. 2012;151(6):1243-55. Epub 2012/12/12. doi: 10.1016/j.cell.2012.10.045. PubMed PMID: 23217708; PubMed Central PMCID: PMCPMC3678556.
18. Batista PJ, Ruby JG, Claycomb JM, Chiang R, Fahlgren N, Kasschau KD, et al. PRG-1 and 21U-RNAs interact to form the piRNA complex required for fertility in C. elegans. Mol Cell. 2008;31(1):67-78. doi: 10.1016/j.molcel.2008.06.002.
19. Gu W, Lee HC, Chaves D, Youngman EM, Pazour GJ, Conte D, Jr., et al. CapSeq and CIP-TAP identify Pol II start sites and reveal capped small RNAs as C. elegans piRNA precursors. Cell. 2012;151(7):1488-500. doi: 10.1016/j.cell.2012.11.023. PubMed PMID: 23260138; PubMed Central PMCID: PMC3581324.
20. Ruby JG, Jan C, Player C, Axtell MJ, Lee W, Nusbaum C, et al. Large-scale sequencing reveals 21U-RNAs and additional microRNAs and endogenous siRNAs in C. elegans. Cell. 2006;127(6):1193-207. doi: 10.1016/j.cell.2006.10.040. PubMed PMID: 17174894.
21. Das PP, Bagijn MP, Goldstein LD, Woolford JR, Lehrbach NJ, Sapetschnig A, et al. Piwi and piRNAs act upstream of an endogenous siRNA pathway to suppress Tc3 transposon mobility in the Caenorhabditis elegans germline. Mol Cell. 2008;31(1):79-90. Epub 2008/06/24. doi: 10.1016/j.molcel.2008.06.003. PubMed PMID: 18571451; PubMed Central PMCID: PMCPMC3353317.
22. Wang G, Reinke V. A C. elegans Piwi, PRG-1, regulates 21U-RNAs during spermatogenesis. Curr Biol. 2008;18(12):861-7. Epub 2008/05/27. doi: 10.1016/j.cub.2008.05.009. PubMed PMID: 18501605; PubMed Central PMCID: PMCPMC2494713.
23. Weick EM, Sarkies P, Silva N, Chen RA, Moss SM, Cording AC, et al. PRDE-1 is a nuclear factor essential for the biogenesis of Ruby motif-dependent piRNAs in C. elegans. Genes Dev. 2014;28(7):783-96. Epub 2014/04/04. doi: 10.1101/gad.238105.114. PubMed PMID: 24696457; PubMed Central PMCID: PMCPMC4015492.
24. Kasper DM, Wang G, Gardner KE, Johnstone TG, Reinke V. The C. elegans SNAPc component SNPC-4 coats piRNA domains and is globally required for piRNA abundance. Developmental cell. 2014;31(2):145-58. doi: 10.1016/j.devcel.2014.09.015. PubMed PMID: 25373775; PubMed Central PMCID: PMC4223638.
25. Goh WS, Seah JW, Harrison EJ, Chen C, Hammell CM, Hannon GJ. A genome-wide RNAi screen identifies factors required for distinct stages of C. elegans piRNA biogenesis. Genes & development. 2014;28(7):797-807. doi: 10.1101/gad.235622.113. PubMed PMID: 24696458; PubMed Central PMCID: PMC4015493.
26. Weng C, Kosalka J, Berkyurek AC, Stempor P, Feng X, Mao H, et al. The USTC co-opts an ancient machinery to drive piRNA transcription in C. elegans. Genes Dev.

2019;33(1-2):90-102. Epub 2018/12/21. doi: 10.1101/gad.319293.118. PubMed PMID: 30567997; PubMed Central PMCID: PMCPMC6317315.
27. Kamminga LM, van Wolfswinkel JC, Luteijn MJ, Kaaij LJ, Bagijn MP, Sapetschnig A, et al. Differential impact of the HEN1 homolog HENN-1 on 21U and 26G RNAs in the germline of Caenorhabditis elegans. PLoS genetics. 2012;8(7):e1002702. doi: 10.1371/journal.pgen.1002702. PubMed PMID: 22829772; PubMed Central PMCID: PMC3400576.
28. Montgomery TA, Rim YS, Zhang C, Dowen RH, Phillips CM, Fischer SE, et al. PIWI associated siRNAs and piRNAs specifically require the Caenorhabditis elegans HEN1 ortholog henn-1. PLoS genetics. 2012;8(4):e1002616. doi: 10.1371/journal.pgen.1002616. PubMed PMID: 22536158; PubMed Central PMCID: PMC3334881.
29. Tang W, Tu S, Lee HC, Weng Z, Mello CC. The RNase PARN-1 Trims piRNA 3' Ends to Promote Transcriptome Surveillance in C. elegans. Cell. 2016;164(5):974-84. Epub 2016/02/27. doi: 10.1016/j.cell.2016.02.008. PubMed PMID: 26919432; PubMed Central PMCID: PMCPMC4785802.
30. Billi AC, Alessi AF, Khivansara V, Han T, Freeberg M, Mitani S, et al. The Caenorhabditis elegans HEN1 ortholog, HENN-1, methylates and stabilizes select subclasses of germline small RNAs. PLoS Genet. 2012;8(4):e1002617. doi: 10.1371/journal.pgen.1002617.
31. Gu W, Shirayama M, Conte D, Jr., Vasale J, Batista PJ, Claycomb JM, et al. Distinct argonaute-mediated 22G-RNA pathways direct genome surveillance in the C. elegans germline. Molecular cell. 2009;36(2):231-44. doi: 10.1016/j.molcel.2009.09.020. PubMed PMID: 19800275; PubMed Central PMCID: PMC2776052.
32. Maniar JM, Fire AZ. EGO-1, a C. elegans RdRP, modulates gene expression via production of mRNA-templated short antisense RNAs. Curr Biol. 2011;21(6):449-59. Epub 2011/03/15. doi: 10.1016/j.cub.2011.02.019. PubMed PMID: 21396820; PubMed Central PMCID: PMCPMC3073447.
33. Shen EZ, Chen H, Ozturk AR, Tu S, Shirayama M, Tang W, et al. Identification of piRNA Binding Sites Reveals the Argonaute Regulatory Landscape of the C. elegans Germline. Cell. 2018;172(5):937-51 e18. Epub 2018/02/20. doi: 10.1016/j.cell.2018.02.002. PubMed PMID: 29456082; PubMed Central PMCID: PMCPMC5905434.
34. Zhang D, Tu S, Stubna M, Wu WS, Huang WC, Weng Z, et al. The piRNA targeting rules and the resistance to piRNA silencing in endogenous genes. Science. 2018;359(6375):587-92. Epub 2018/02/09. doi: 10.1126/science.aao2840. PubMed PMID: 29420292; PubMed Central PMCID: PMCPMC5939965.
35. Ashe A, Sapetschnig A, Weick EM, Mitchell J, Bagijn MP, Cording AC, et al. piRNAs can trigger a multigenerational epigenetic memory in the germline of C. elegans. Cell. 2012;150(1):88-99. Epub 2012/06/29. doi: 10.1016/j.cell.2012.06.018. PubMed PMID: 22738725; PubMed Central PMCID: PMCPMC3464430.
36. Lee HC, Gu W, Shirayama M, Youngman E, Conte D, Jr., Mello CC. C. elegans piRNAs mediate the genome-wide surveillance of germline transcripts. Cell. 2012;150(1):78-87. doi: 10.1016/j.cell.2012.06.016. PubMed PMID: 22738724; PubMed Central PMCID: PMC3410639.

37. Shirayama M, Seth M, Lee HC, Gu W, Ishidate T, Conte D, Jr., et al. piRNAs initiate an epigenetic memory of nonself RNA in the C. elegans germline. Cell. 2012;150(1):65-77. doi: 10.1016/j.cell.2012.06.015. PubMed PMID: 22738726; PubMed Central PMCID: PMC3597741.
38. Bagijn MP, Goldstein LD, Sapetschnig A, Weick EM, Bouasker S, Lehrbach NJ, et al. Function, targets, and evolution of Caenorhabditis elegans piRNAs. Science. 2012;337(6094):574-8. doi: 10.1126/science.1220952. PubMed PMID: 22700655.
39. Buckley BA, Burkhart KB, Gu SG, Spracklin G, Kershner A, Fritz H, et al. A nuclear Argonaute promotes multigenerational epigenetic inheritance and germline immortality. Nature. 2012;489(7416):447-51. Epub 2012/07/20. doi: 10.1038/nature11352. PubMed PMID: 22810588; PubMed Central PMCID: PMCPMC3509936.
40. Reed KJ, Svendsen JM, Brown KC, Montgomery BE, Marks TN, Vijayasarathy T, et al. Widespread roles for piRNAs and WAGO-class siRNAs in shaping the germline transcriptome of Caenorhabditis elegans. Nucleic acids research. 2020;48(4):1811-27. Epub 2019/12/25. doi: 10.1093/nar/gkz1178. PubMed PMID: 31872227; PubMed Central PMCID: PMCPMC7038979.
41. Barucci G, Cornes E, Singh M, Li B, Ugolini M, Samolygo A, et al. Small-RNA-mediated transgenerational silencing of histone genes impairs fertility in piRNA mutants. Nature cell biology. 2020;22(2):235-45. Epub 2020/02/06. doi: 10.1038/s41556-020-0462-7. PubMed PMID: 32015436; PubMed Central PMCID: PMCPMC7272227.
42. Wahba L, Hansen L, Fire AZ. An essential role for the piRNA pathway in regulating the ribosomal RNA pool in C. elegans. Developmental cell. 2021;56(16):2295-312 e6. Epub 2021/08/14. doi: 10.1016/j.devcel.2021.07.014. PubMed PMID: 34388368; PubMed Central PMCID: PMCPMC8387450.
43. Montgomery BE, Vijayasarathy T, Marks TN, Cialek CA, Reed KJ, Montgomery TA. Dual roles for piRNAs in promoting and preventing gene silencing in C. elegans. Cell Rep. 2021;37(10):110101. Epub 2021/12/09. doi: 10.1016/j.celrep.2021.110101. PubMed PMID: 34879267.
44. Stein LD, Bao Z, Blasiar D, Blumenthal T, Brent MR, Chen N, et al. The genome sequence of Caenorhabditis briggsae: a platform for comparative genomics. PLoS biology. 2003;1(2):E45. doi: 10.1371/journal.pbio.0000045. PubMed PMID: 14624247; PubMed Central PMCID: PMC261899.
45. Shi Z, Montgomery TA, Qi Y, Ruvkun G. High-throughput sequencing reveals extraordinary fluidity of miRNA, piRNA, and siRNA pathways in nematodes. Genome Res. 2013;23(3):497-508. Epub 2013/02/01. doi: 10.1101/gr.149112.112. PubMed PMID: 23363624; PubMed Central PMCID: PMCPMC3589538.
46. Wedeles CJ, Wu MZ, Claycomb JM. Protection of Germline Gene Expression by the C. elegans Argonaute CSR-1. Developmental cell. 2013. doi: 10.1016/j.devcel.2013.11.016. PubMed PMID: 24360783.
47. Seth M, Shirayama M, Gu W, Ishidate T, Conte D, Jr., Mello CC. The C. elegans CSR-1 Argonaute Pathway Counteracts Epigenetic Silencing to Promote Germline Gene Expression. Developmental cell. 2013. doi: 10.1016/j.devcel.2013.11.014. PubMed PMID: 24360782.
48. Pastore B, Hertz HL, Price IF, Tang W. pre-piRNA trimming and 2'-O-methylation protect piRNAs from 3' tailing and degradation in C. elegans. Cell Rep.

2021;36(9):109640. Epub 2021/09/02. doi: 10.1016/j.celrep.2021.109640. PubMed PMID: 34469728; PubMed Central PMCID: PMCPMC8459939.
49. Bartel DP. Metazoan MicroRNAs. Cell. 2018;173(1):20-51. Epub 2018/03/24. doi: 10.1016/j.cell.2018.03.006. PubMed PMID: 29570994; PubMed Central PMCID: PMCPMC6091663.
50. Beltran T, Barroso C, Birkle TY, Stevens L, Schwartz HT, Sternberg PW, et al. Comparative Epigenomics Reveals that RNA Polymerase II Pausing and Chromatin Domain Organization Control Nematode piRNA Biogenesis. Dev Cell. 2019;48(6):793-810 e6. Epub 2019/02/05. doi: 10.1016/j.devcel.2018.12.026. PubMed PMID: 30713076; PubMed Central PMCID: PMCPMC6436959.
51. Carninci P, Sandelin A, Lenhard B, Katayama S, Shimokawa K, Ponjavic J, et al. Genome-wide analysis of mammalian promoter architecture and evolution. Nat Genet. 2006;38(6):626-35. Epub 2006/04/29. doi: 10.1038/ng1789. PubMed PMID: 16645617.
52. Carninci P, Kasukawa T, Katayama S, Gough J, Frith MC, Maeda N, et al. The transcriptional landscape of the mammalian genome. Science. 2005;309(5740):1559-63. Epub 2005/09/06. doi: 10.1126/science.1112014. PubMed PMID: 16141072.
53. Boyer LA, Latek RR, Peterson CL. The SANT domain: a unique histone-tail-binding module? Nat Rev Mol Cell Biol. 2004;5(2):158-63. Epub 2004/03/26. doi: 10.1038/nrm1314. PubMed PMID: 15040448.
54. Mello C, Fire A. DNA transformation. Methods Cell Biol. 1995;48:451-82. Epub 1995/01/01. PubMed PMID: 8531738.
55. Gou L-T, Dai P, Yang J-H, Xue Y, Hu Y-P, Zhou Y, et al. Pachytene piRNAs instruct massive mRNA elimination during late spermiogenesis. Cell Res. 2014;24(6):680-700. doi: 10.1038/cr.2014.41.
56. Goh WSS, Falciatori I, Tam OH, Burgess R, Meikar O, Kotaja N, et al. piRNA-directed cleavage of meiotic transcripts regulates spermatogenesis. Genes Dev. 2015;29(10):1032-44. doi: 10.1101/gad.260455.115.
57. Simon M, Sarkies P, Ikegami K, Doebley AL, Goldstein LD, Mitchell J, et al. Reduced insulin/IGF-1 signaling restores germ cell immortality to Caenorhabditis elegans Piwi mutants. Cell Rep. 2014;7(3):762-73. Epub 2014/04/29. doi: 10.1016/j.celrep.2014.03.056. PubMed PMID: 24767993; PubMed Central PMCID: PMCPMC4049074.
58. Prasad A, Croydon-Sugarman MJ, Murray RL, Cutter AD. Temperature-dependent fecundity associates with latitude in Caenorhabditis briggsae. Evolution. 2011;65(1):52-63. Epub 2010/08/25. doi: 10.1111/j.1558-5646.2010.01110.x. PubMed PMID: 20731713.
59. Begasse ML, Leaver M, Vazquez F, Grill SW, Hyman AA. Temperature Dependence of Cell Division Timing Accounts for a Shift in the Thermal Limits of C. elegans and C. briggsae. Cell Rep. 2015;10(5):647-53. Epub 2015/02/11. doi: 10.1016/j.celrep.2015.01.006. PubMed PMID: 25660015.
60. Maduro MF. 20 Years of unc-119 as a transgene marker. Worm. 2015;4(3):e1046031. Epub 2015/10/03. doi: 10.1080/21624054.2015.1046031. PubMed PMID: 26430568; PubMed Central PMCID: PMCPMC4588520.
61. Heestand B, Simon M, Frenk S, Titov D, Ahmed S. Transgenerational Sterility of Piwi Mutants Represents a Dynamic Form of Adult Reproductive Diapause. Cell Rep.

2018;23(1):156-71. Epub 2018/04/05. doi: 10.1016/j.celrep.2018.03.015. PubMed PMID: 29617657; PubMed Central PMCID: PMCPMC5918633.
62. Lant B, Derry WB. Fluorescent visualization of germline apoptosis in living Caenorhabditis elegans. Cold Spring Harb Protoc. 2014;2014(4):420-7. Epub 2014/04/03. doi: 10.1101/pdb.prot080226. PubMed PMID: 24692492.
63. Claycomb JM, Batista PJ, Pang KM, Gu W, Vasale JJ, van Wolfswinkel JC, et al. The Argonaute CSR-1 and its 22G-RNA cofactors are required for holocentric chromosome segregation. Cell. 2009;139(1):123-34. Epub 2009/10/07. doi: 10.1016/j.cell.2009.09.014. PubMed PMID: 19804758; PubMed Central PMCID: PMCPMC2766185.
64. Tu S, Wu MZ, Wang J, Cutter AD, Weng Z, Claycomb JM. Comparative functional characterization of the CSR-1 22G-RNA pathway in Caenorhabditis nematodes. Nucleic Acids Res. 2015;43(1):208-24. Epub 2014/12/17. doi: 10.1093/nar/gku1308. PubMed PMID: 25510497; PubMed Central PMCID: PMCPMC4288196.
65. Miller LM, Plenefisch JD, Casson LP, Meyer BJ. xol-1: a gene that controls the male modes of both sex determination and X chromosome dosage compensation in C. elegans. Cell. 1988;55(1):167-83. PubMed PMID: 3167975.
66. Helwak A, Kudla G, Dudnakova T, Tollervey D. Mapping the human miRNA interactome by CLASH reveals frequent noncanonical binding. Cell. 2013;153(3):654-65. doi: 10.1016/j.cell.2013.03.043. PubMed PMID: 23622248; PubMed Central PMCID: PMCPMC3650559.
67. Merritt C, Rasoloson D, Ko D, Seydoux G. 3' UTRs are the primary regulators of gene expression in the C. elegans germline. Current biology : CB. 2008;18(19):1476-82. doi: 10.1016/j.cub.2008.08.013. PubMed PMID: 18818082; PubMed Central PMCID: PMC2585380.
68. Jan CH, Friedman RC, Ruby JG, Bartel DP. Formation, regulation and evolution of Caenorhabditis elegans 3'UTRs. Nature. 2011;469(7328):97-101. doi: 10.1038/nature09616. PubMed PMID: 21085120; PubMed Central PMCID: PMCPMC3057491.
69. Tabach Y, Billi AC, Hayes GD, Newman MA, Zuk O, Gabel H, et al. Identification of small RNA pathway genes using patterns of phylogenetic conservation and divergence. Nature. 2013;493(7434):694-8. Epub 2013/02/01. doi: 10.1038/nature11779. PubMed PMID: 23364702; PubMed Central PMCID: PMCPMC3762460.
70. Newman MA, Ji F, Fischer SEJ, Anselmo A, Sadreyev RI, Ruvkun G. The surveillance of pre-mRNA splicing is an early step in C. elegans RNAi of endogenous genes. Genes Dev. 2018;32(9-10):670-81. Epub 2018/05/10. doi: 10.1101/gad.311514.118. PubMed PMID: 29739806; PubMed Central PMCID: PMCPMC6004069.
71. Akay A, Di Domenico T, Suen KM, Nabih A, Parada GE, Larance M, et al. The Helicase Aquarius/EMB-4 Is Required to Overcome Intronic Barriers to Allow Nuclear RNAi Pathways to Heritably Silence Transcription. Dev Cell. 2017;42(3):241-55 e6. Epub 2017/08/09. doi: 10.1016/j.devcel.2017.07.002. PubMed PMID: 28787591; PubMed Central PMCID: PMCPMC5554785.
72. Makeyeva YV, Shirayama M, Mello CC. Cues from mRNA splicing prevent default Argonaute silencing in C. elegans. Dev Cell. 2021;56(18):2636-48 e4. Epub 2021/09/22.

doi: 10.1016/j.devcel.2021.08.022. PubMed PMID: 34547227; PubMed Central PMCID: PMCPMC8693449.
73. Khurana JS, Wang J, Xu J, Koppetsch BS, Thomson TC, Nowosielska A, et al. Adaptation to P element transposon invasion in Drosophila melanogaster. Cell. 2011;147(7):1551-63. Epub 2011/12/27. doi: 10.1016/j.cell.2011.11.042. PubMed PMID: 22196730; PubMed Central PMCID: PMCPMC3246748.
74. Gebert D, Neubert LK, Lloyd C, Gui J, Lehmann R, Teixeira FK. Large Drosophila germline piRNA clusters are evolutionarily labile and dispensable for transposon regulation. Mol Cell. 2021;81(19):3965-78 e5. Epub 2021/08/06. doi: 10.1016/j.molcel.2021.07.011. PubMed PMID: 34352205; PubMed Central PMCID: PMCPMC8516431.
75. Dumesic PA, Natarajan P, Chen C, Drinnenberg IA, Schiller BJ, Thompson J, et al. Stalled spliceosomes are a signal for RNAi-mediated genome defense. Cell. 2013;152(5):957-68. Epub 2013/02/19. doi: 10.1016/j.cell.2013.01.046. PubMed PMID: 23415457; PubMed Central PMCID: PMCPMC3645481.
76. Le Hir H, Sauliere J, Wang Z. The exon junction complex as a node of post-transcriptional networks. Nat Rev Mol Cell Biol. 2016;17(1):41-54. Epub 2015/12/17. doi: 10.1038/nrm.2015.7. PubMed PMID: 26670016.
77. Phillips CM, Montgomery TA, Breen PC, Ruvkun G. MUT-16 promotes formation of perinuclear mutator foci required for RNA silencing in the C. elegans germline. Genes Dev. 2012;26(13):1433-44. Epub 2012/06/21. doi: 10.1101/gad.193904.112. PubMed PMID: 22713602; PubMed Central PMCID: PMCPMC3403012.
78. Shukla A, Yan J, Pagano DJ, Dodson AE, Fei Y, Gorham J, et al. poly(UG)-tailed RNAs in genome protection and epigenetic inheritance. Nature. 2020;582(7811):283-8. Epub 2020/06/06. doi: 10.1038/s41586-020-2323-8. PubMed PMID: 32499657.
79. Sarkies P, Selkirk ME, Jones JT, Blok V, Boothby T, Goldstein B, et al. Ancient and novel small RNA pathways compensate for the loss of piRNAs in multiple independent nematode lineages. PLoS Biol. 2015;13(2):e1002061/1-e/20. doi: 10.1371/journal.pbio.1002061.
80. Roovers EF, Rosenkranz D, Mahdipour M, Han CT, He N, Chuva de Sousa Lopes SM, et al. Piwi proteins and piRNAs in mammalian oocytes and early embryos. Cell Rep. 2015;10(12):2069-82. Epub 2015/03/31. doi: 10.1016/j.celrep.2015.02.062. PubMed PMID: 25818294.
81. Lewis SH, Quarles KA, Yang Y, Tanguy M, Frezal L, Smith SA, et al. Pan-arthropod analysis reveals somatic piRNAs as an ancestral defence against transposable elements. Nat Ecol Evol. 2018;2(1):174-81. Epub 2017/12/06. doi: 10.1038/s41559-017-0403-4. PubMed PMID: 29203920; PubMed Central PMCID: PMCPMC5732027.
82. Jinek M, Chylinski K, Fonfara I, Hauer M, Doudna JA, Charpentier E. A programmable dual-RNA-guided DNA endonuclease in adaptive bacterial immunity. Science. 2012;337(6096):816-21. Epub 2012/06/30. doi: 10.1126/science.1225829. PubMed PMID: 22745249; PubMed Central PMCID: PMCPMC6286148.
83. Brenner S. The genetics of Caenorhabditis elegans. Genetics. 1974;77(1):71-94. Epub 1974/05/01. PubMed PMID: 4366476; PubMed Central PMCID: PMCPMC1213120.
84. Frokjaer-Jensen C, Davis MW, Hopkins CE, Newman BJ, Thummel JM, Olesen SP, et al. Single-copy insertion of transgenes in Caenorhabditis elegans. Nat Genet.

2008;40(11):1375-83. Epub 2008/10/28. doi: 10.1038/ng.248. PubMed PMID: 18953339; PubMed Central PMCID: PMCPMC2749959.
85. Kim H, Ishidate T, Ghanta KS, Seth M, Conte D, Jr., Shirayama M, et al. A co-CRISPR strategy for efficient genome editing in Caenorhabditis elegans. Genetics. 2014;197(4):1069-80. Epub 2014/06/01. doi: 10.1534/genetics.114.166389. PubMed PMID: 24879462; PubMed Central PMCID: PMCPMC4125384.
86. Li L, Dai H, Nguyen AP, Gu W. A convenient strategy to clone small RNA and mRNA for high-throughput sequencing. Rna. 2020;26(2):218-27. Epub 2019/11/23. doi: 10.1261/rna.071605.119. PubMed PMID: 31754076; PubMed Central PMCID: PMCPMC6961543.
87. Langmead B, Trapnell C, Pop M, Salzberg SL. Ultrafast and memory-efficient alignment of short DNA sequences to the human genome. Genome Biol. 2009;10(3):R25. Epub 2009/03/06. doi: 10.1186/gb-2009-10-3-r25. PubMed PMID: 19261174; PubMed Central PMCID: PMCPMC2690996.
88. Neph S, Kuehn MS, Reynolds AP, Haugen E, Thurman RE, Johnson AK, et al. BEDOPS: high-performance genomic feature operations. Bioinformatics. 2012;28(14):1919-20. Epub 2012/05/12. doi: 10.1093/bioinformatics/bts277. PubMed PMID: 22576172; PubMed Central PMCID: PMCPMC3389768.
89. Quinlan AR, Hall IM. BEDTools: a flexible suite of utilities for comparing genomic features. Bioinformatics. 2010;26(6):841-2. Epub 2010/01/30. doi: 10.1093/bioinformatics/btq033. PubMed PMID: 20110278; PubMed Central PMCID: PMCPMC2832824.
90. Jurka J, Kapitonov VV, Pavlicek A, Klonowski P, Kohany O, Walichiewicz J. Repbase Update, a database of eukaryotic repetitive elements. Cytogenetic and Genome Research. 2005;110(1-4):462-7. doi: 10.1159/000084979.
91. Bailey TL, Boden M, Buske FA, Frith M, Grant CE, Clementi L, et al. MEME SUITE: tools for motif discovery and searching. Nucleic Acids Res. 2009;37(Web Server issue):W202-8. Epub 2009/05/22. doi: 10.1093/nar/gkp335. PubMed PMID: 19458158; PubMed Central PMCID: PMCPMC2703892.
92. Zhang D, Tu S, Stubna M, Wu W-S, Huang W-C, Weng Z, et al. The piRNA targeting rules and the resistance to piRNA silencing in endogenous genes. Science. 2018;359(6375):587-92. doi: doi:10.1126/science.aao2840.
93. Li H, Durbin R. Fast and accurate short read alignment with Burrows-Wheeler transform. Bioinformatics. 2009;25(14):1754-60. Epub 2009/05/20. doi: 10.1093/bioinformatics/btp324. PubMed PMID: 19451168; PubMed Central PMCID: PMCPMC2705234.
94. Hadley Wickham RF, Lionel Henry, Kirill Müller. dplyr: A Grammar of Data Manipulation. 2022.

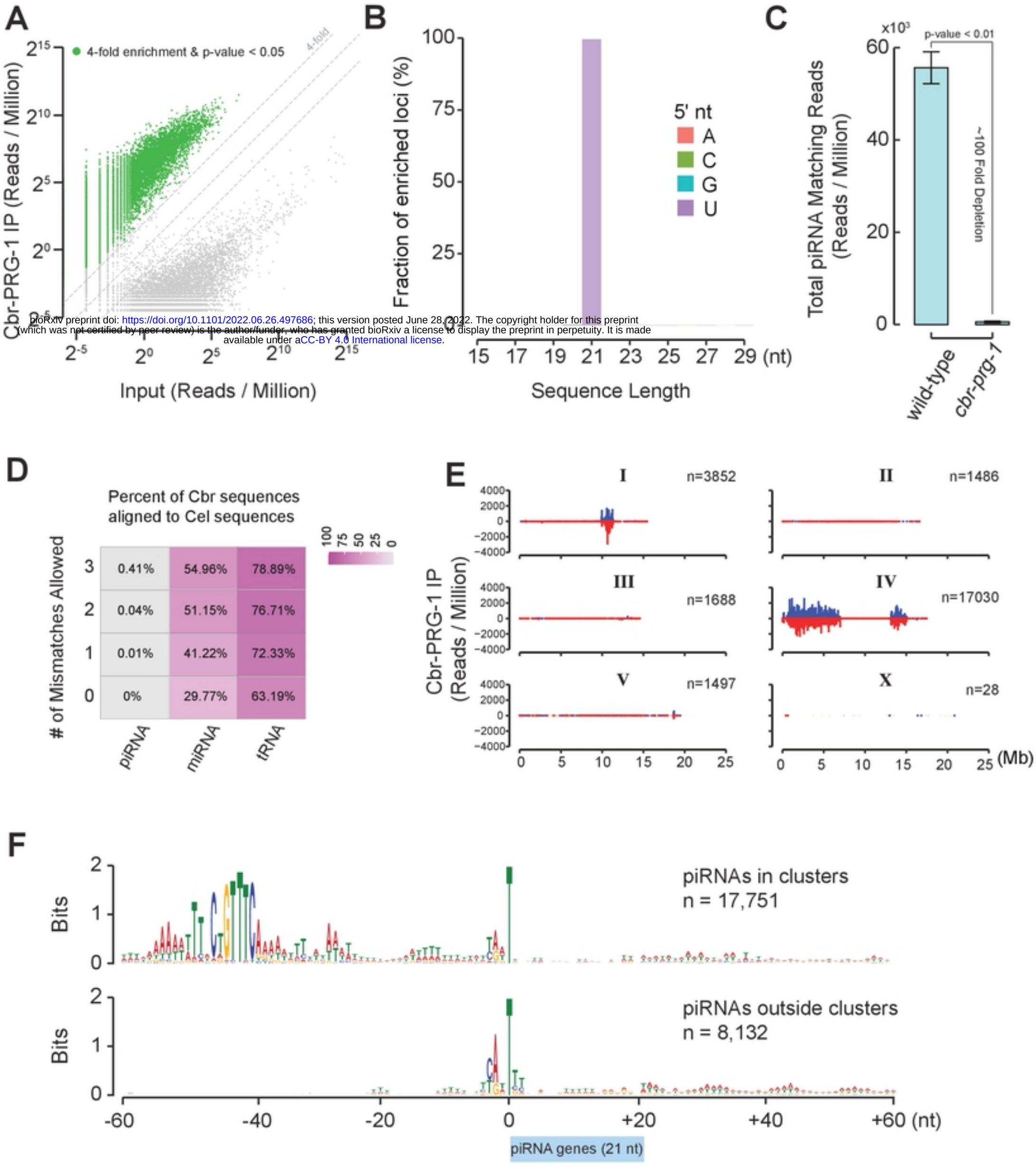

Figure 1

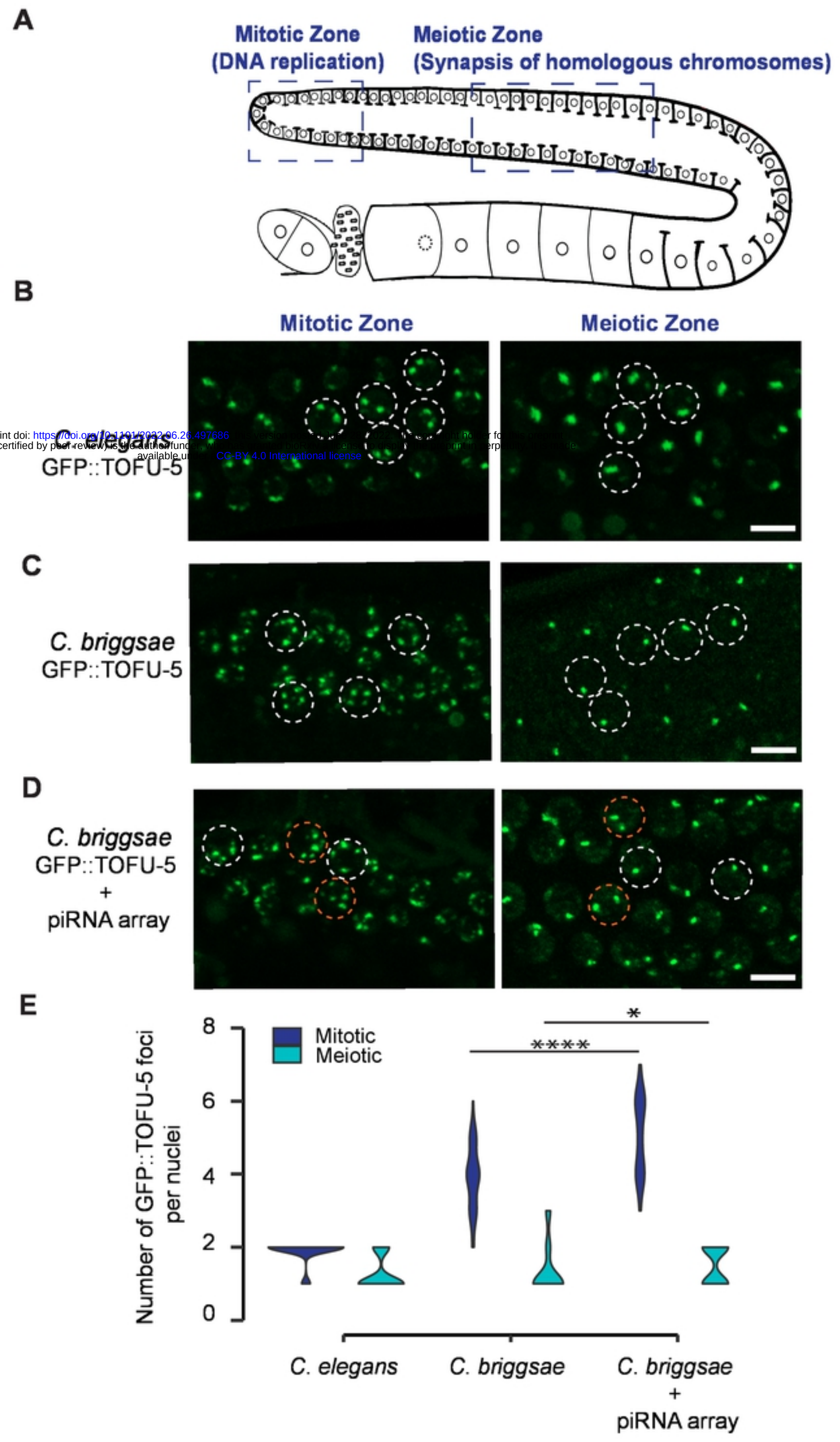

Figure 2

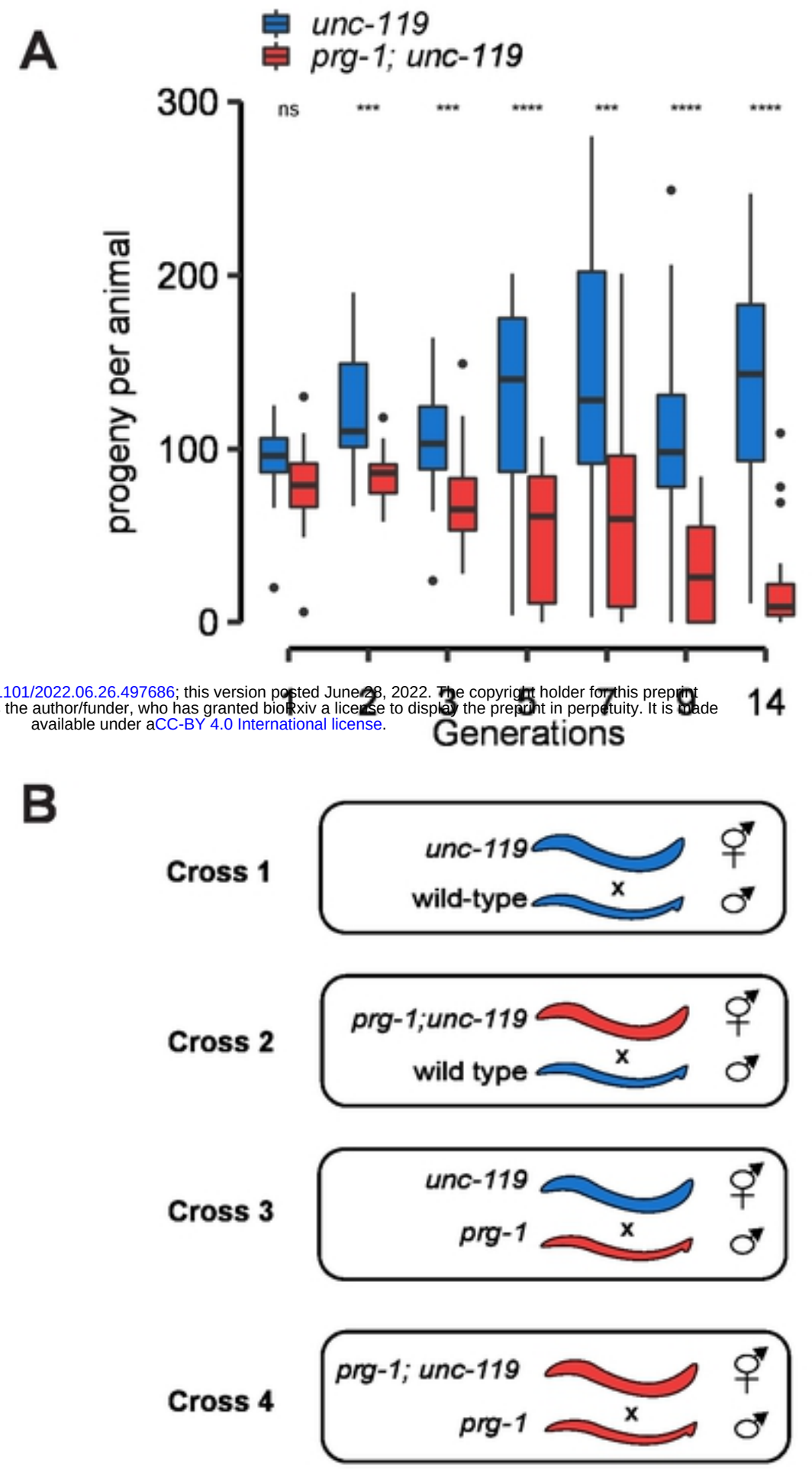

Figure 3

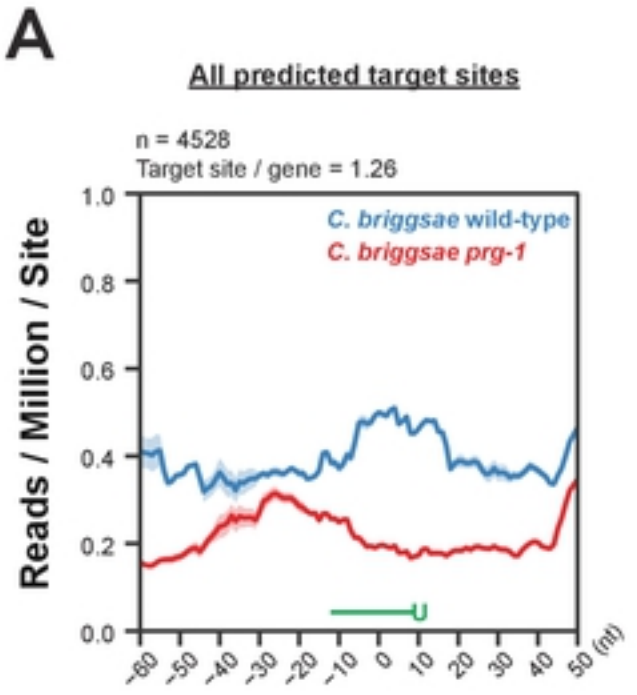

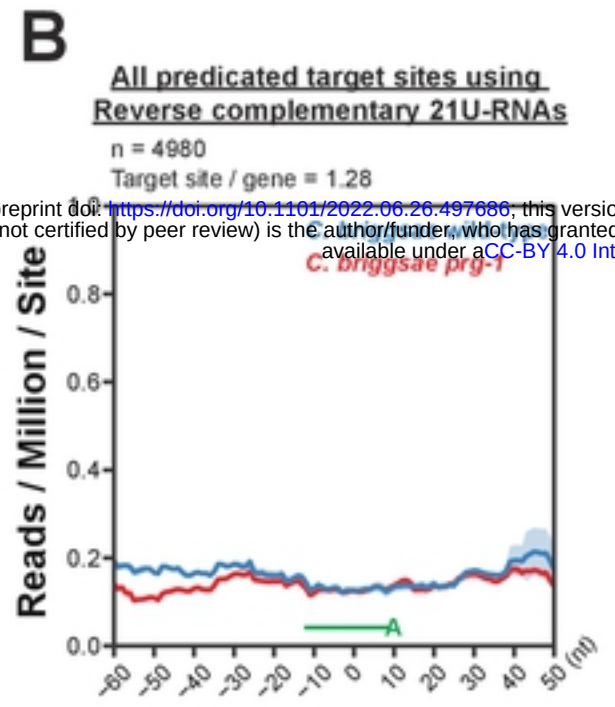

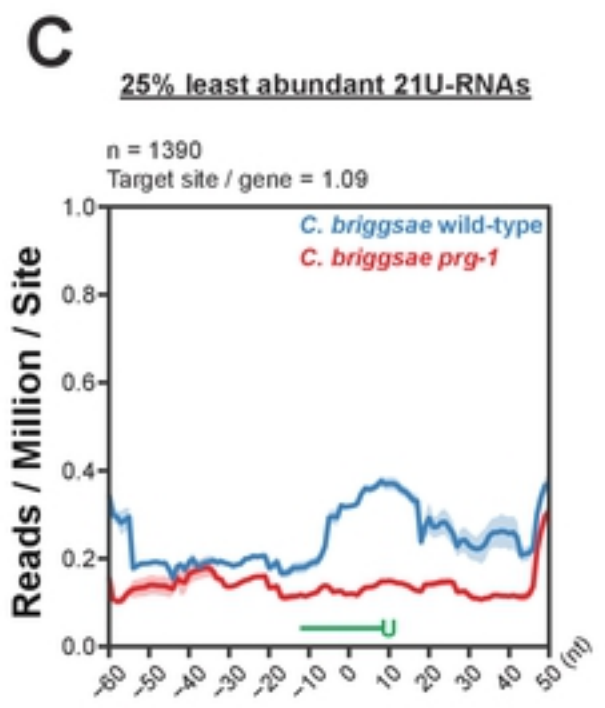

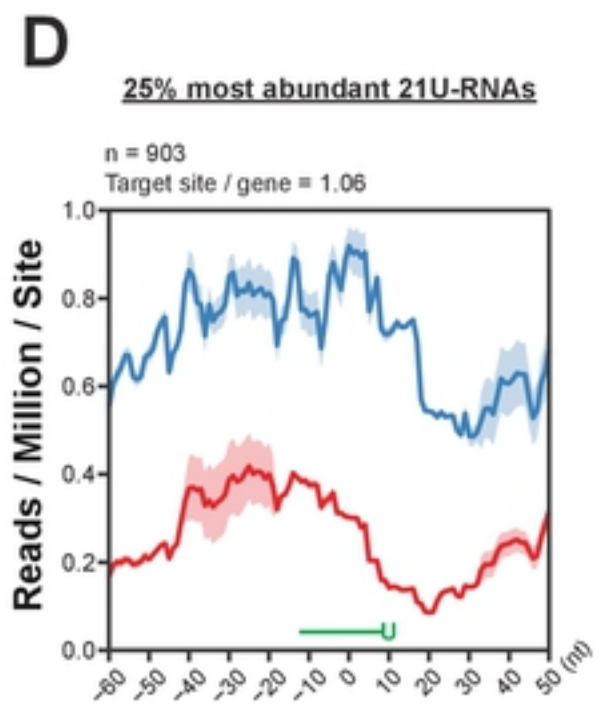

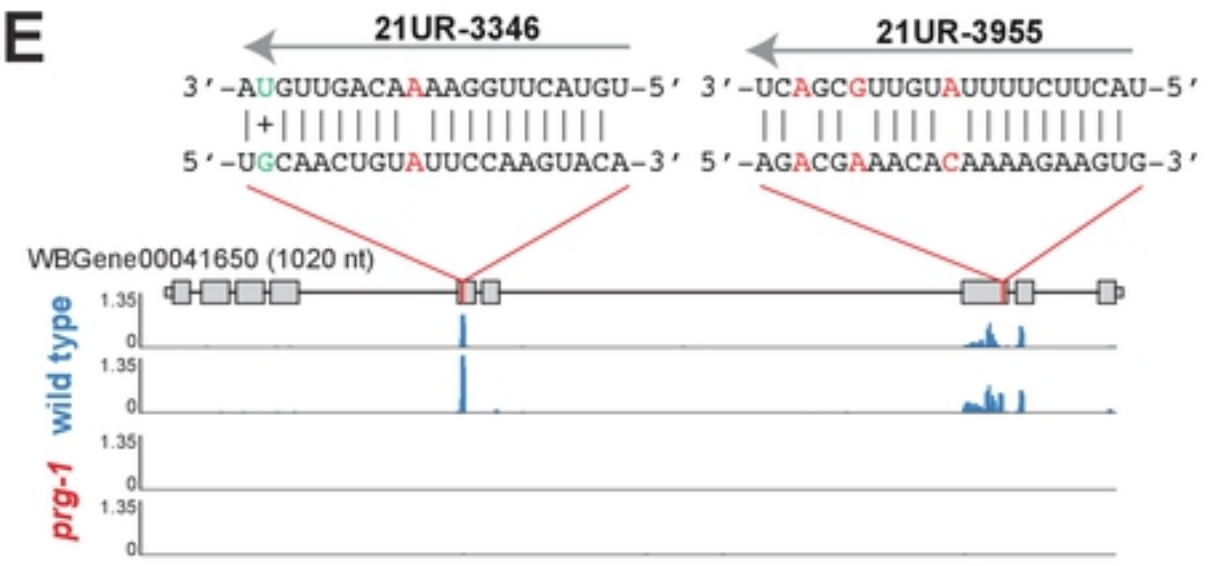

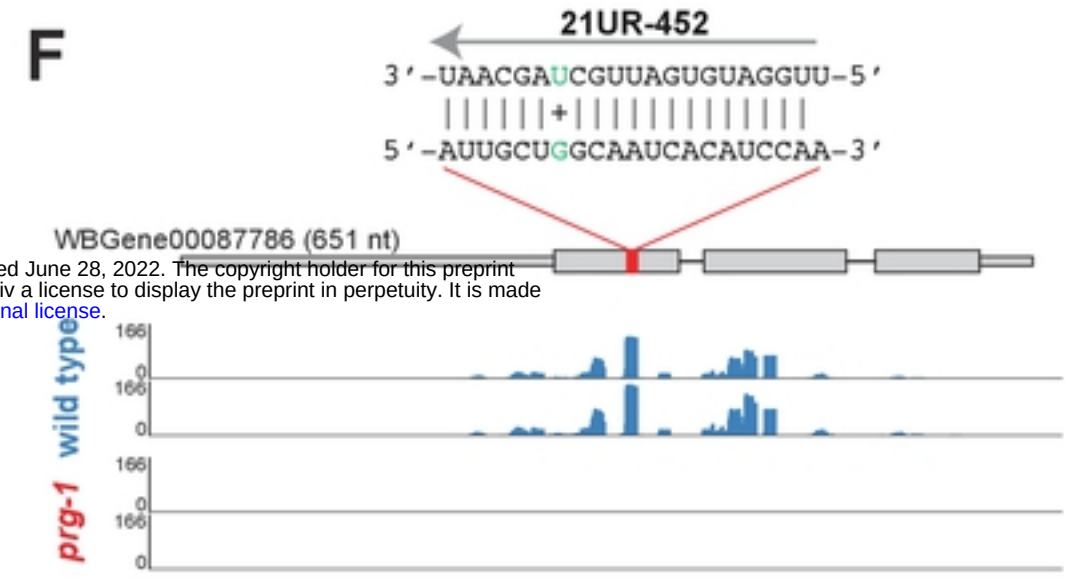

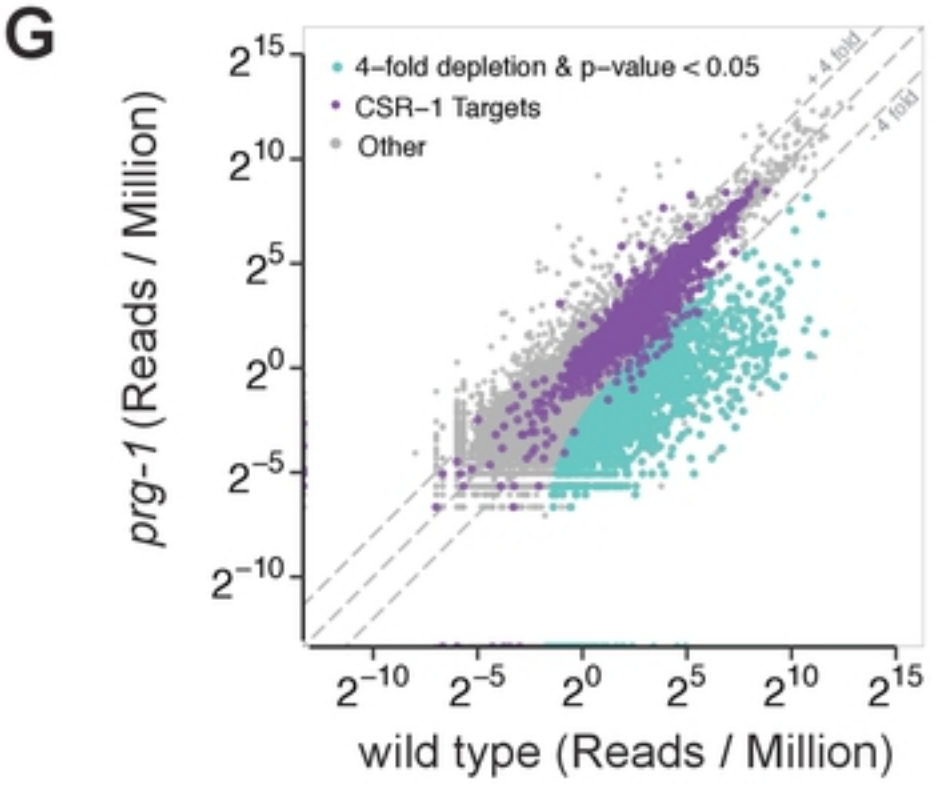

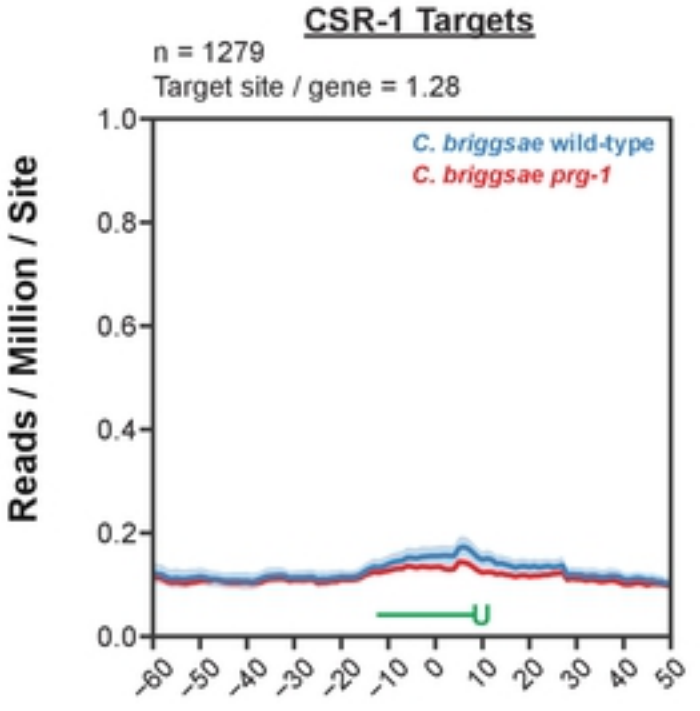

Figure 4

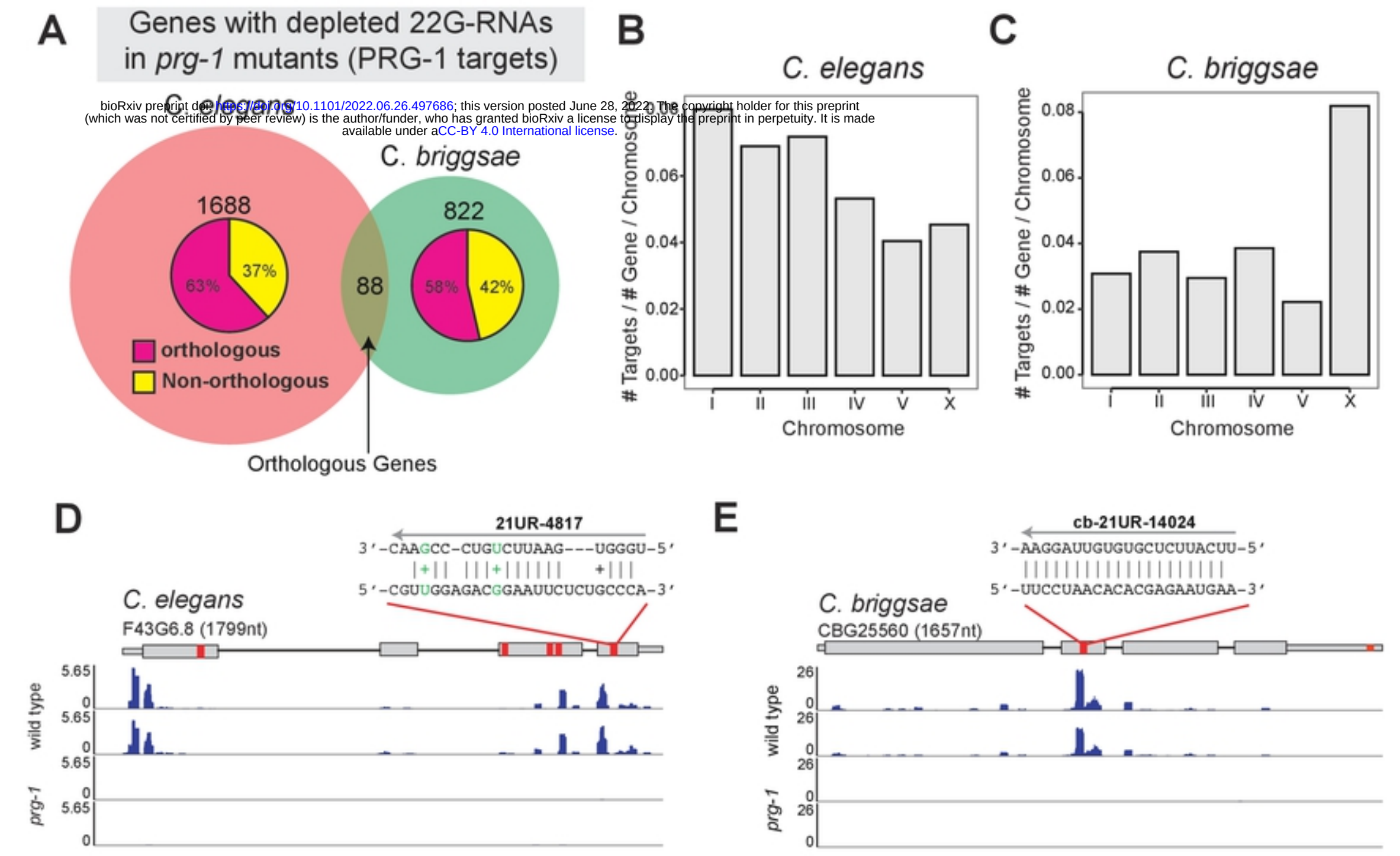

Figure 5

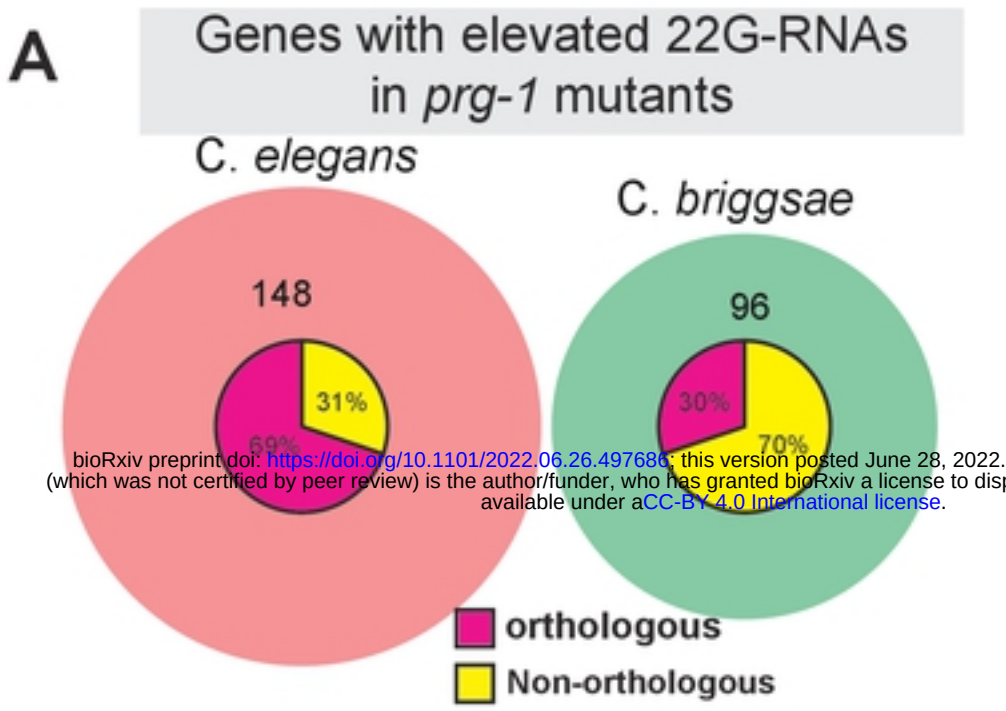

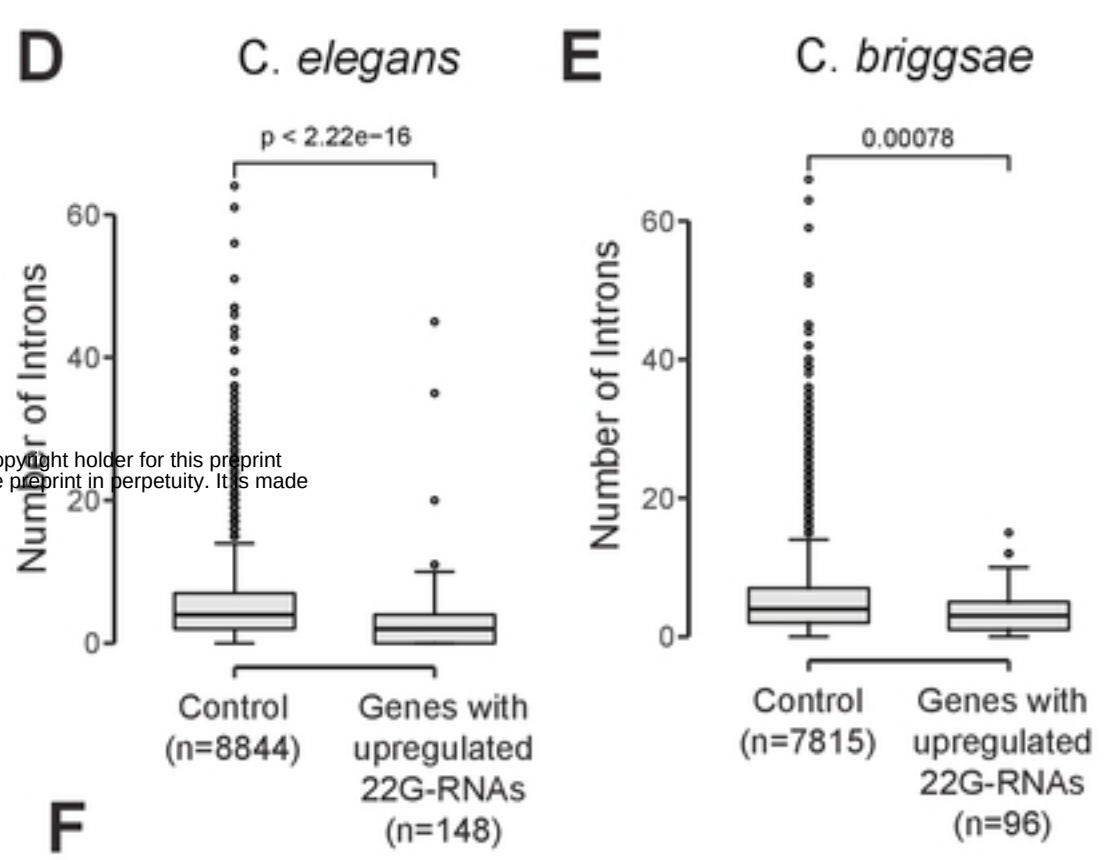

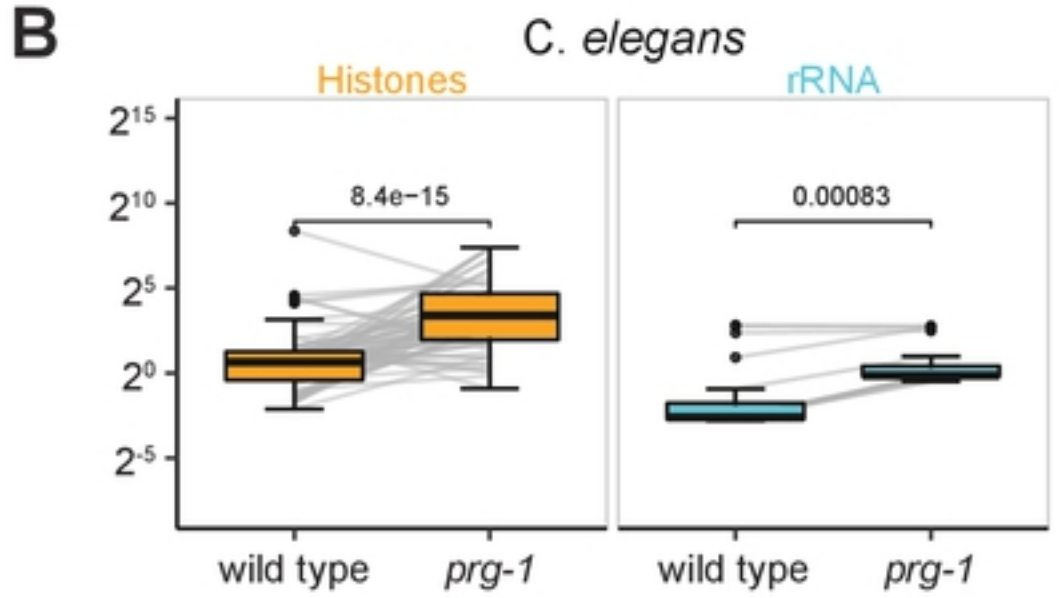

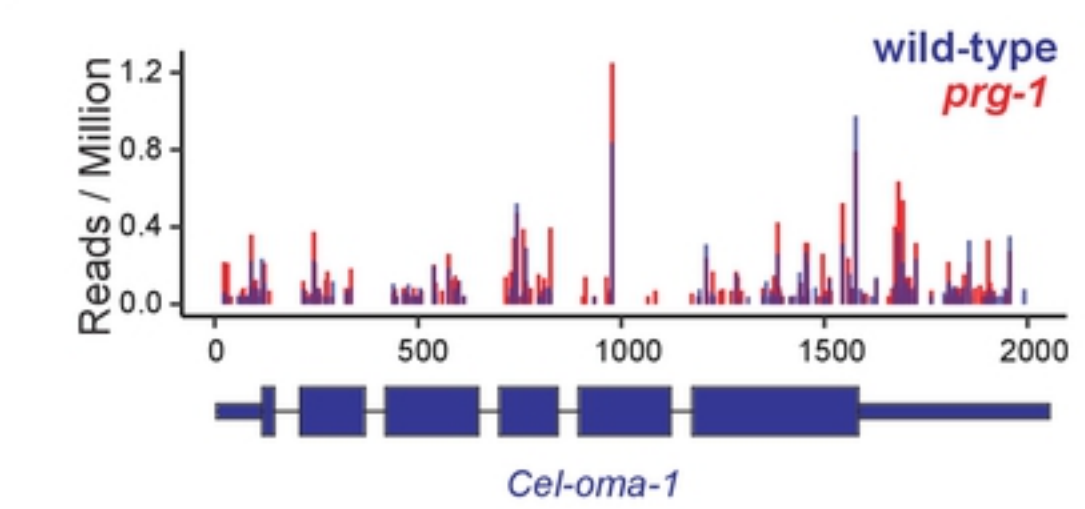

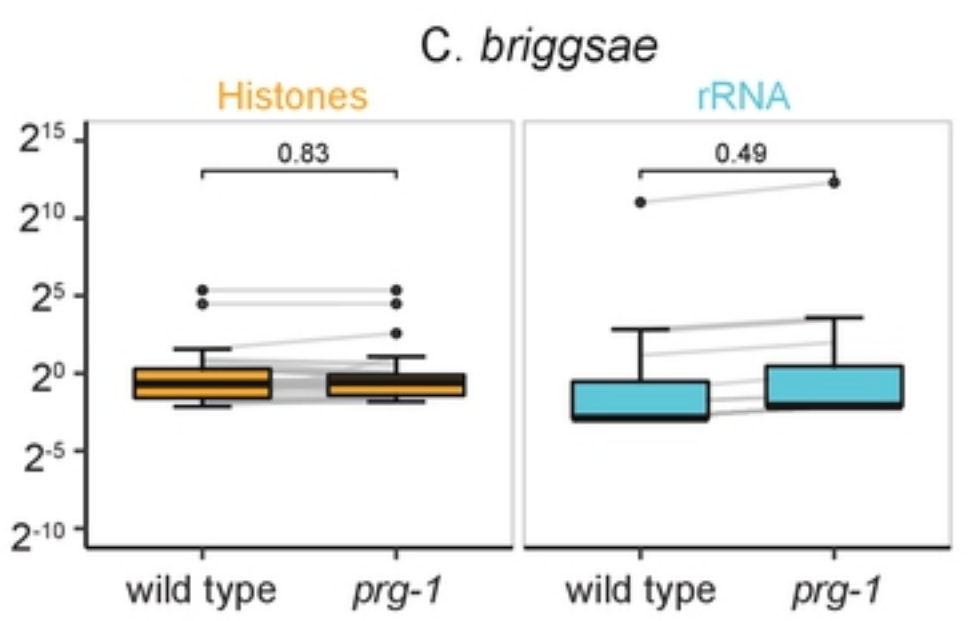

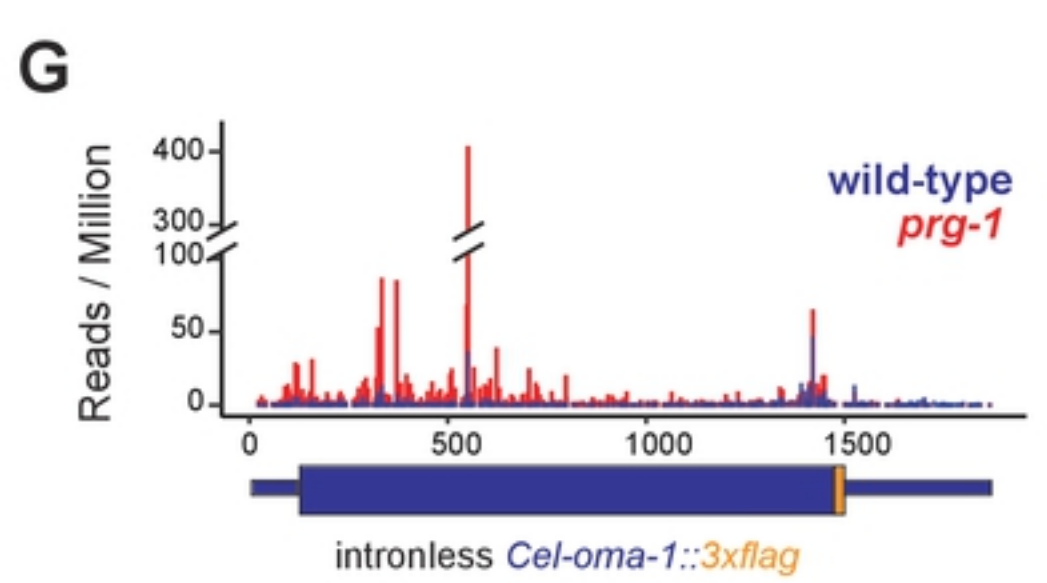

Figure 6

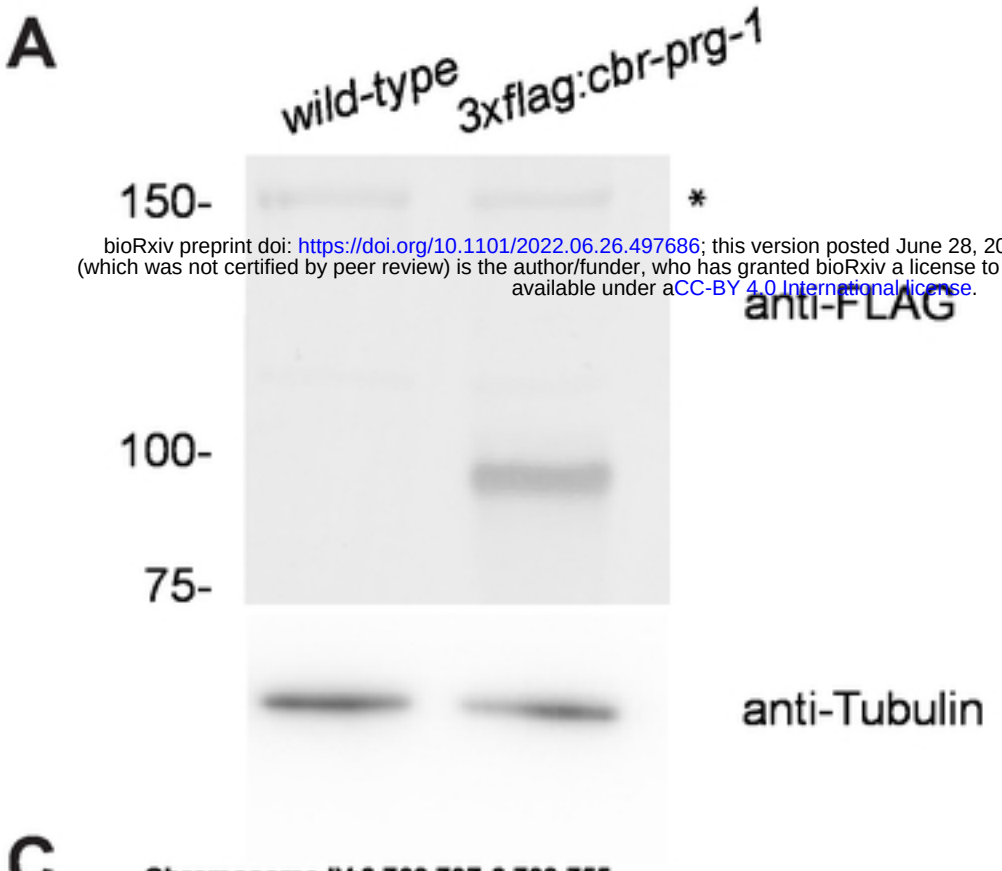

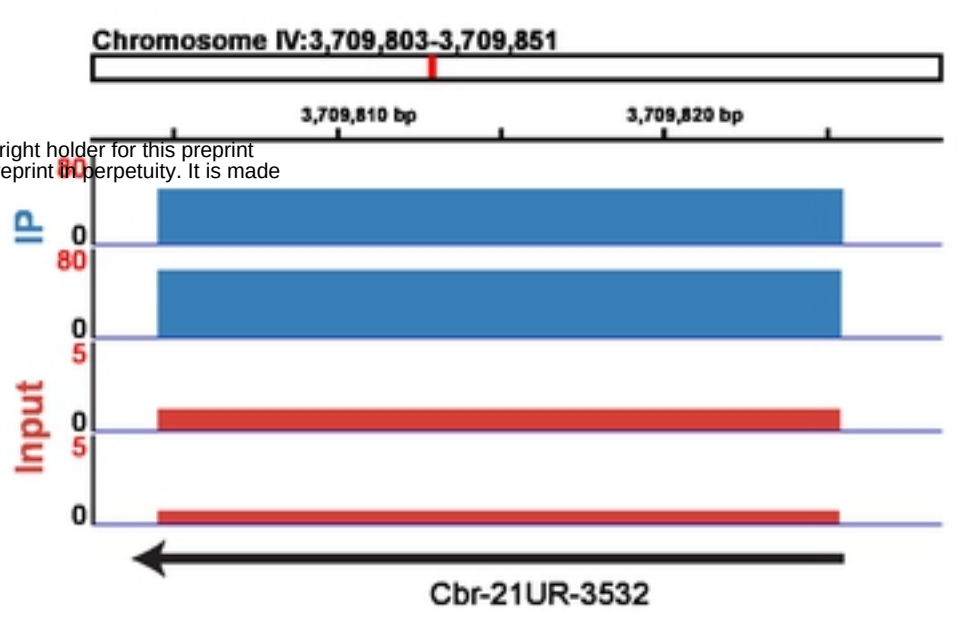

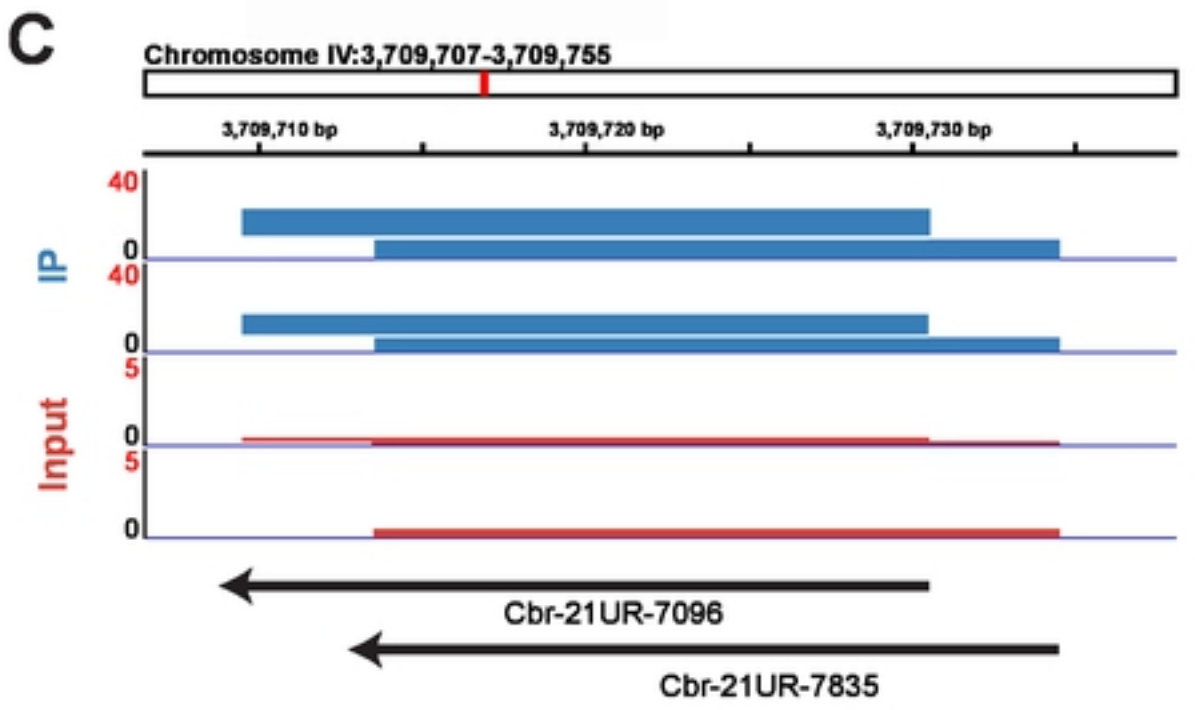

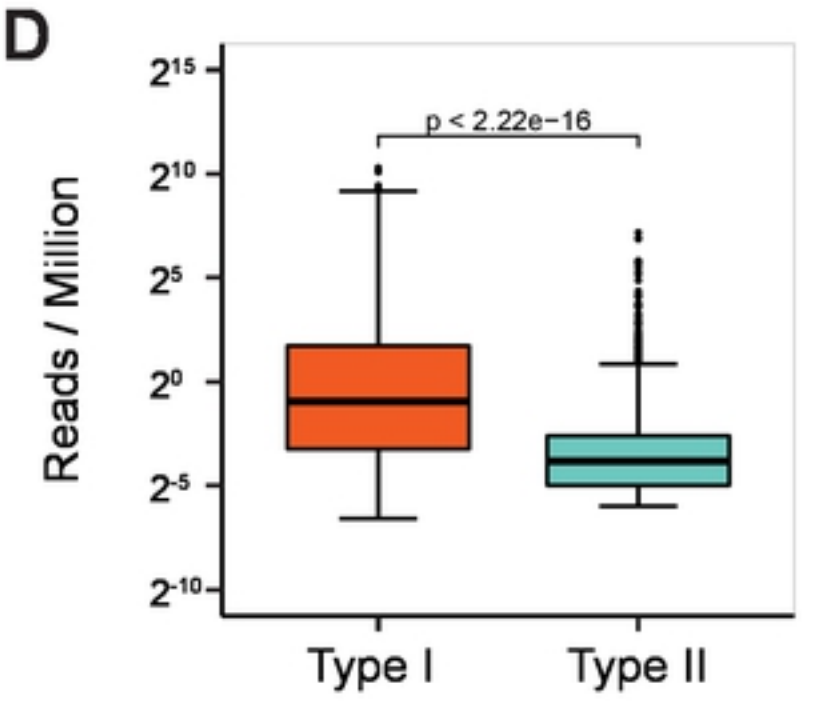

Figure S1

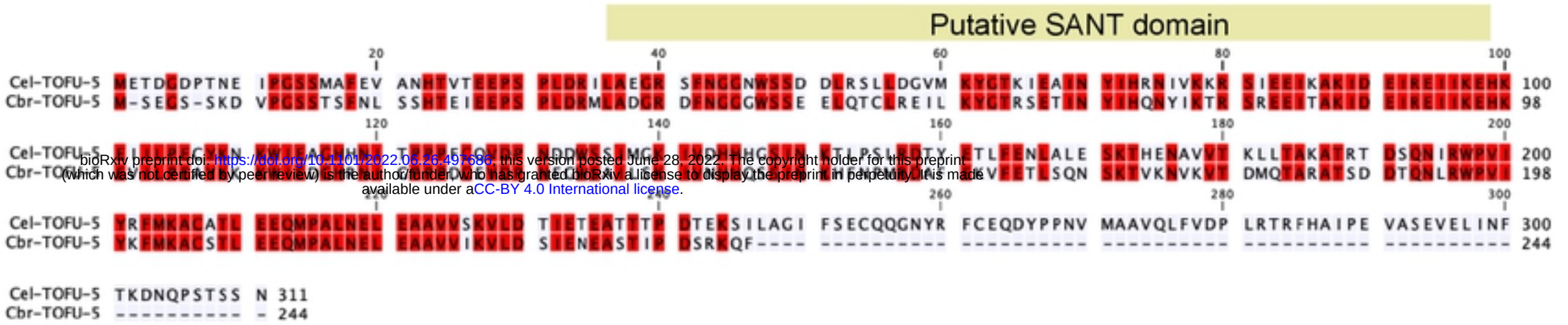

Figure S2

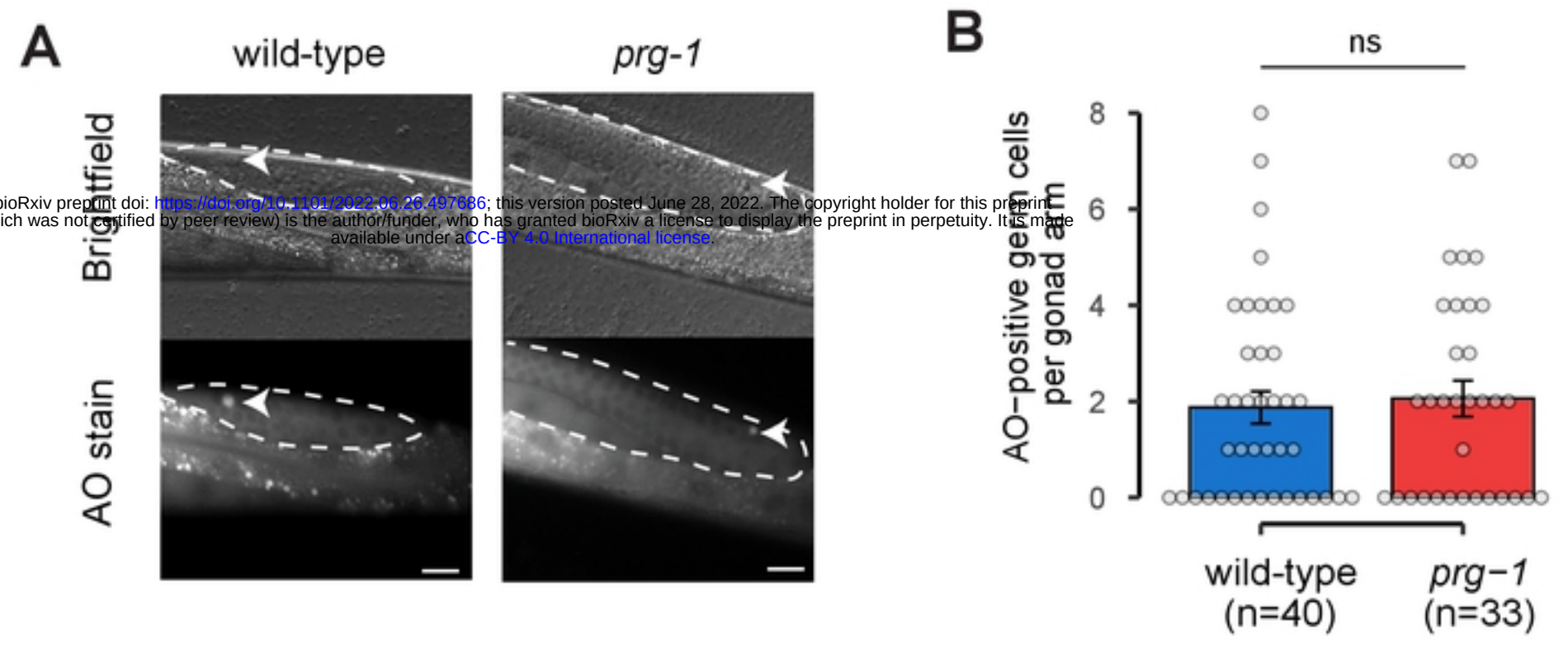

Figure S3

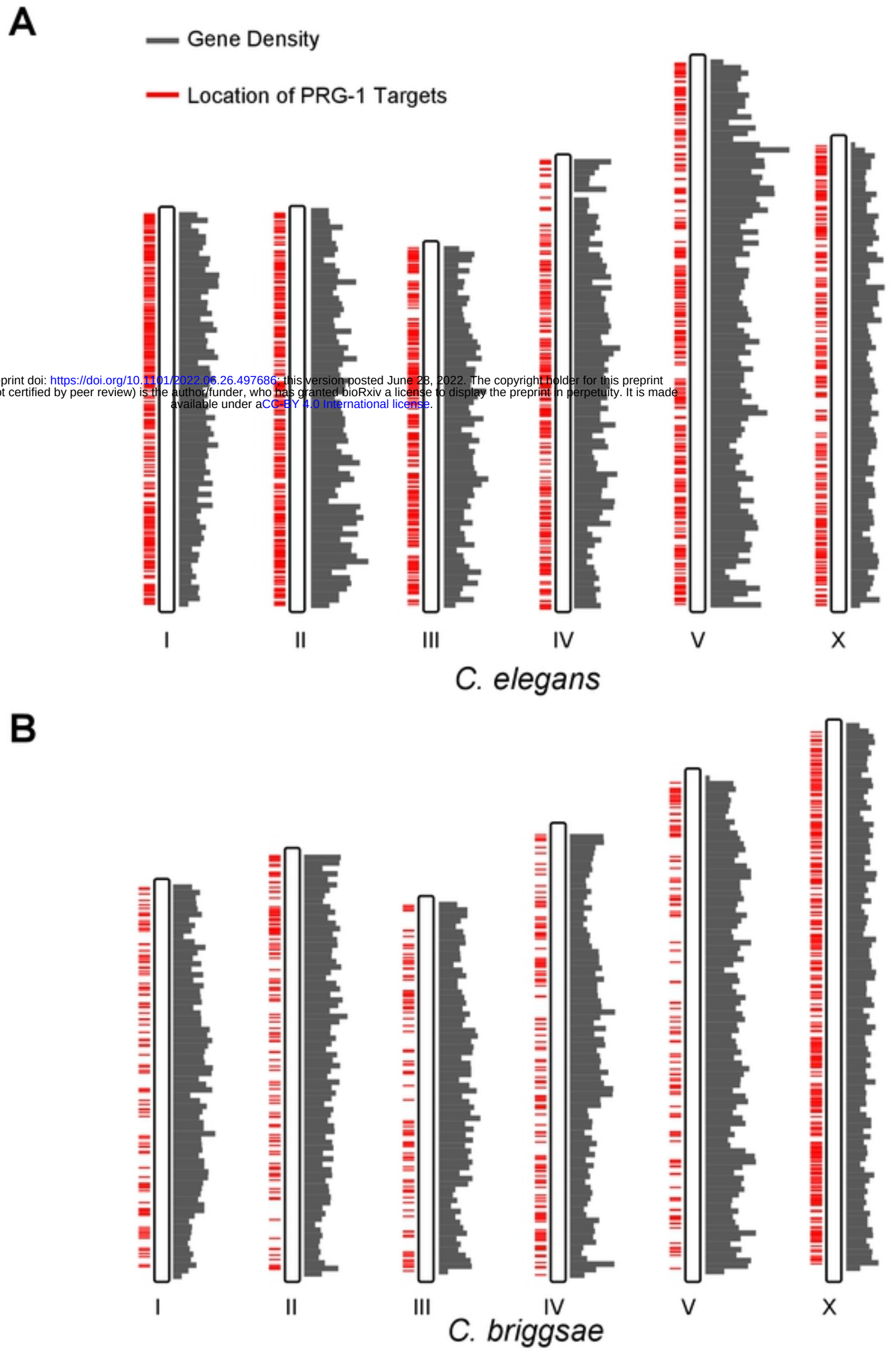

Figure S4

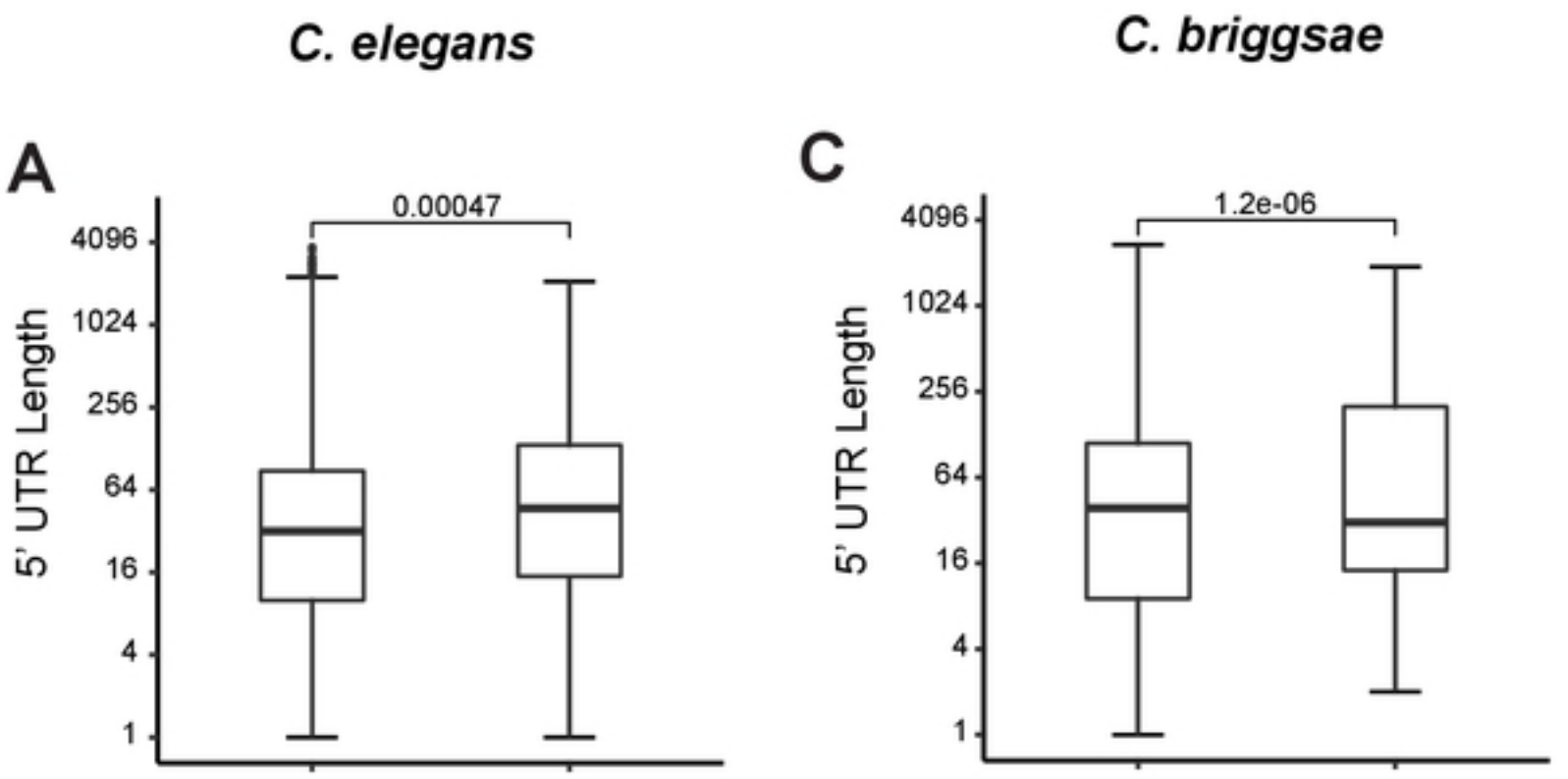

Figure S5